

Feature Transportation Improves Graph Neural Networks

Moshe Eliasof^{1,2*}, Eldad Haber³, Eran Treister²

¹ Department of Applied Mathematics and Theoretical Physics, University of Cambridge, United Kingdom

² Department of Computer Science, Ben-Gurion University of the Negev, Israel

³ Department of Earth, Ocean, and Atmospheric Sciences, University of British Columbia, Canada
me532@cam.ac.uk, ehaber@eoas.ubc.ca, erant@cs.bgu.ac.il

Abstract

Graph neural networks (GNNs) have shown remarkable success in learning representations for graph-structured data. However, GNNs still face challenges in modeling complex phenomena that involve feature transportation. In this paper, we propose a novel GNN architecture inspired by Advection-Diffusion-Reaction systems, called ADR-GNN. Advection models feature transportation, while diffusion captures the local smoothing of features, and reaction represents the non-linear transformation between feature channels. We provide an analysis of the qualitative behavior of ADR-GNN, that shows the benefit of combining advection, diffusion, and reaction. To demonstrate its efficacy, we evaluate ADR-GNN on real-world node classification and spatio-temporal datasets, and show that it improves or offers competitive performance compared to state-of-the-art networks.

1 Introduction

Recently, GNNs have been linked to ordinary and partial differential equations (ODEs and PDEs) in a series of works (Zhuang et al. 2020; Chamberlain et al. 2021; Eliasof, Haber, and Treister 2021; Rusch et al. 2022a; Wang et al. 2022; Giovanni et al. 2023; Gravina, Bacciu, and Gallicchio 2023). These works propose to view GNN layers as the time discretization of ODEs and PDEs, and as such they offer both theoretical and practical advantages. First, ODE and PDE based models allow to reason about the behavior of existing GNNs. For instance, as suggested in (Chamberlain et al. 2021), it is possible to view GCN (Kipf and Welling 2017) and GAT (Veličković et al. 2018) as discretizations of the non-linear heat equation. This observation helps to analyze and understand the oversmoothing phenomenon in GNNs (Nt and Maehara 2019; Oono and Suzuki 2020; Cai and Wang 2020). Second, ODE and PDE based GNNs pave the path to the construction and design of GNNs that satisfy desired properties, such as energy-preservation (Eliasof, Haber, and Treister 2021; Rusch et al. 2022a), attraction and repulsion forces modeling (Wang et al. 2022; Giovanni et al. 2023), anti-symmetry (Gravina, Bacciu, and Gallicchio 2023), as well as reaction-diffusion systems (Choi

et al. 2022). Nonetheless, the aforementioned architectures still rely on controlled diffusion or wave propagation, as well as non-linear pointwise convolutions. Therefore, as discussed in (Rusch, Bronstein, and Mishra 2023), while there are methods that can alleviate oversmoothing, they may lack expressiveness. We now provide a simple example, known as the graph node feature transportation task (LeVeque 1990), where diffusion, wave propagation, and reaction networks may fail. In this task, the goal is to gather the node information (i.e., features) from several nodes to a single node. Clearly, no diffusion process can express or model such a phenomenon, because diffusion spreads and smooths, rather than transports information (Evans 1998; Ascher 2008). Likewise, a wave-propagation approach cannot express such a phenomenon, because it lacks directionality (Ascher 2008), which is required for this task. An instance of this problem is illustrated in Figure 1, where we show the source and target node features, and the learned advection weights that can achieve the desired target. Later, in Figure 2, we show that popular operators such as diffusion or reaction cannot model the transition from the source to the target node features, while advection can. Furthermore, the concept of advection appears in many real-world problems and data, such as traffic-flow and-control (Betts 2001), quantity transportation in computational biology (Uys 2009), and rainfall forecasting (Seed 2003). Motivated by the previously discussed observations and examples, we propose, in addition to learning and combining diffusion and reaction terms, to develop a learnable, neural *advection* term, also known as a *transportation* term (Evans 1998; Ascher 2008; LeVeque 1990), that is suited to model feature transportation from the data in a task driven fashion. The resulting architecture, called *ADR-GNN*, can therefore express various phenomena, from advection, diffusion, to pointwise reactions, as well as their compositions.

Contributions. The contributions of this paper are three-fold. (1) We develop a novel graph neural advection operator that is mass preserving, stable, and consistent with continuous advection PDEs. This operator enables the modeling of phenomena that involve feature transportation on graphs by learning the direction of the transportation. (2) We propose ADR-GNN, a GNN based on learnable advection-diffusion-reaction (ADR) systems, that can express a wide range of phenomena, including learned directional information flow,

*Work done while being a Ph.D. student at Ben-Gurion University of the Negev.

Copyright © 2024, Association for the Advancement of Artificial Intelligence (www.aaai.org). All rights reserved.

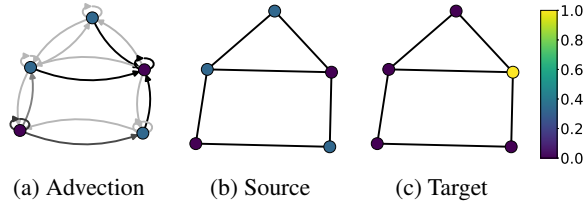


Figure 1: An example of node feature transportation on a graph. Applying the advection weights in (a) to the source (b), yields the target (c). Darker edge colors in (a) indicate greater advection weights.

diffusion, and pointwise reactions. (3) We demonstrate the efficacy of ADR-GNN on node classification, and spatio-temporal forecasting datasets, achieving improved or competitive results compared to state-of-the-art models.

2 Related Work

Advection-Diffusion-Reaction. An Advection Diffusion Reaction system is a mathematical model that describes the simultaneous existence of three processes: (1) the advection (transport) of information in a medium, (2) the diffusion (smoothing) of information within that medium, and (3) pointwise (self) reactions. These systems are used to study and model a wide range of physical, chemical, and biological phenomena. For example, ADR systems can be utilized to track and estimate the location of fish swarms (Adam and Sibert 2004), modeling ecological trends (Cosner 2014), and the modeling of turbulent flames in supernovae (Khokhlov 1995). However, the aforementioned works rely on a low-dimensional, hand-crafted, non-neural ADR system to be determined, typically by trial and error, often requiring a domain expert. In contrast, in this paper we propose to learn the ADR system for various graph types and tasks.

Graph Neural Networks as Dynamical Systems. Adopting the interpretation of convolutional neural networks (CNNs) as discretizations of ODEs and PDEs (Ruthotto and Haber 2020; Chen et al. 2018b; Zhang et al. 2019a) to GNNs, works like GODE (Zhuang et al. 2020), GRAND (Chamberlain et al. 2021), PDE-GCN_D (Eliasof, Haber, and Treister 2021), GRAND++ (Thorpe et al. 2022) and others, propose to view GNN layers as time steps in the integration of the non-linear heat equation, allowing to control the diffusion (smoothing) in the network, to understand oversmoothing (Nt and Maehara 2019; Oono and Suzuki 2020; Cai and Wang 2020) in GNNs. Thus, works like (Chien et al. 2021; Luan et al. 2020, 2022; Giovanni et al. 2023) propose to utilize a *learnable* diffusion term, thereby alleviating oversmoothing. Other architectures like PDE-GCN_M (Eliasof, Haber, and Treister 2021) and GraphCON (Rusch et al. 2022a) propose to mix diffusion and oscillatory processes (e.g., based on the wave equation) to avoid oversmoothing by introducing a feature energy preservation mechanism. Nonetheless, as noted in (Rusch, Bronstein, and Mishra 2023), besides alleviating oversmoothing, it is also important to design GNN architectures with im-

proved expressiveness. Recent examples of such networks are (Gravina, Bacciu, and Gallicchio 2023) that propose an anti-symmetric GNN to alleviate over-squashing (Alon and Yahav 2021), and (Wang et al. 2022; Choi et al. 2022) that formulate a reaction-diffusion GNN to enable non-trivial pattern growth. In this paper, we build on the properties of ADR PDEs, that in addition to modeling diffusive and reactive processes, also allow to capture advective processes such as the transportation of node features.

On another note, CNNs and GNNs are also used to accelerate PDE solvers (Raissi 2018; Long et al. 2018; Li et al. 2020; Brandstetter, Worrall, and Welling 2022; Saadat et al. 2022), as well as to generate (Sanchez-Gonzalez et al. 2019) and compute (Belbute-Peres, Economou, and Kolter 2020) physical simulations. In this paper, we focus on the view of GNNs as the discretization of ADR PDEs, rather than using GNNs to solve PDEs.

Advection on Graphs. Advection is a term used in Physics to describe the transport of a substance in a medium. In the context of graphs, advection is used to express the transport of information (features) on the graph nodes. The underlying process of advection is described by a continuous PDE, and several graph discretization techniques (Chapman and Chapman 2015; Hošek and Volek 2019) are available. The advection operator has shown its effectiveness in classical (i.e., non-neural) graph methods, from blood-vessel simulations (Deepa Maheshvare, Raha, and Pal 2022), to traffic flow prediction (Borovitskiy et al. 2021). In this paper, we develop a neural advection operator that is combined with neural diffusion and reaction operators, called ADR-GNN.

3 Method

In this section, we first describe the general outline of a continuous ADR system in Section 3.1, and present its graph discrete analog, named *ADR-GNN* in Section 3.2. We discuss ADR-GNN components in detail in Sections 3.3-3.4.

Notations. We define a graph by $\mathcal{G} = (\mathcal{V}, \mathcal{E})$, where \mathcal{V} is a set of n nodes and $\mathcal{E} \subseteq \mathcal{V} \times \mathcal{V}$ is a set of m edges. We denote the 1-hop neighborhood of the i -th node by \mathcal{N}_i , and the node features by $\mathbf{U} \in \mathbb{R}^{n \times c}$, where c is the number of features. The symmetric graph Laplacian reads $\mathbf{L} = \mathbf{D} - \mathbf{A}$, and the symmetric normalized Laplacian is given by $\hat{\mathbf{L}} = \mathbf{D}^{-\frac{1}{2}} \mathbf{L} \mathbf{D}^{-\frac{1}{2}}$, where \mathbf{D} is the degree matrix.

3.1 Continuous Advection-Diffusion-Reaction Systems

The continuous PDE that describes an ADR system is given by:

$$\frac{\partial U}{\partial t} = \underbrace{\nabla \cdot (VU)}_{\text{Advection}} + \underbrace{K \Delta U}_{\text{Diffusion}} + \underbrace{f(U, X, \theta_r)}_{\text{Reaction}}, \quad (1)$$

where $X \in \Omega$, $t \in [0, T]$, accompanied by initial conditions $U(X, t = 0)$ and boundary conditions. Here, $U(X, t) = [u_1(X, t), \dots, u_c(X, t)] : \mathbb{R}^{\Omega \times [0, T]} \rightarrow \mathbb{R}^c$ is a density function, written as a vector of scalar functions $u_s(X, t)$, $s = 1, \dots, c$, that depend on the initial location X and time t . The spatial domain Ω can be \mathbb{R}^d or a manifold $\mathcal{M} \subseteq \mathbb{R}^d$.

From a neural network perspective, u_s is referred to as a channel, interacting with other channels. The left-hand side of Equation (1) is a time derivative that represents the change in features in time, as discussed in Section 2. The right-hand side includes three terms:

- **Advection.** Here, V denotes a velocity function that transports the density U in space, and $\nabla \cdot$ is the divergence operator.
- **Diffusion.** We denote the continuous Laplacian operator by Δ . The Laplacian is scaled with a diagonal matrix $K = \text{diag}(\kappa_1, \dots, \kappa_c) \in \mathbb{R}^{c \times c}$, $\kappa_i \geq 0$ of non-negative diffusion coefficients, each independently applied to its corresponding channel in U .
- **Reaction.** Here, $f(U, X, \theta_r)$ is a non-linear pointwise function parameterized by θ_r .

3.2 Advection-Diffusion-Reaction on Graphs

Equation (1) is defined in the continuum. We now use a graph $\mathcal{G} = (\mathcal{V}, \mathcal{E})$ to discretize Ω . The nodes \mathcal{V} can be regarded as a discretization of X , that is, the i -th node is located in \mathbf{X}_i , and the edges \mathcal{E} represent the topology of Ω . Then, the *spatial*, graph discretization of Equation (1) is:

$$\frac{d\mathbf{U}(t)}{dt} = \mathbf{DIV}(\mathbf{V}(\mathbf{U}(t), t; \boldsymbol{\theta}_a(t)) \mathbf{U}(t)) \quad (2a)$$

$$- \hat{\mathbf{L}}\mathbf{U}(t)\mathbf{K}(t; \boldsymbol{\theta}_d(t)) + f(\mathbf{U}(t), \mathbf{X}, t; \boldsymbol{\theta}_r(t)),$$

$$\mathbf{U}(0) = \mathbf{U}^{(0)} = g_{in}(\mathbf{X}, \boldsymbol{\theta}_0). \quad (2b)$$

Here, $\mathbf{U}(t) \in \mathbb{R}^{n \times c}$ is a matrix that describes the node features at time t . The advection term depends on the velocity function \mathbf{V} parameterized by learnable weights $\boldsymbol{\theta}_a(t)$. The precise discretization of the advection operator $\mathbf{DIV}(\mathbf{V} \cdot)$ is discussed in Section 3.4. The diffusion is discretized using the symmetric normalized Laplacian¹ $\hat{\mathbf{L}}$ that is scaled with a diagonal matrix with non-negative learnable diffusion coefficients on its diagonal $\mathbf{K}(t; \boldsymbol{\theta}_d(t)) = \text{diag}(\text{hardtanh}(\boldsymbol{\theta}_d(t), 0, 1)) \geq 0$, where $\text{hardtanh}(\boldsymbol{\theta}_d(t), 0, 1)$ clamps each element in $\boldsymbol{\theta}_d \in \mathbb{R}^c$ to be between 0 and 1. The reaction term f from Equation (2a) is a pointwise non-linear function realized by a multilayer-perceptron (MLP) parameterized by learnable weights $\boldsymbol{\theta}_r(t)$. To obtain initial node embedding $\mathbf{U}^{(0)} \in \mathbb{R}^{n \times c}$ from the input features $\mathbf{X} \in \mathbb{R}^{n \times c_{in}}$, we use a fully-connected layer g_{in} in Equation (2b).

In this work we focus on static and temporal node-level tasks, and we note that typically, c , the number of hidden channels of $\mathbf{U}(T) \in \mathbb{R}^{n \times c}$, is different than c_{out} , the number of channels of the target output $\mathbf{Y} \in \mathbb{R}^{n \times c_{out}}$. Therefore the output of neural network, $\tilde{\mathbf{Y}}$, is given by

$$\tilde{\mathbf{Y}} = g_{out}(\mathbf{U}(T), \boldsymbol{\theta}_{out}) \in \mathbb{R}^{n \times c_{out}}, \quad (3)$$

where g_{out} is a fully-connected layer with weights $\boldsymbol{\theta}_{out}$.

The qualitative behavior of ADR-GNN. The ADR-GNN model combines the learning of three powerful terms.

¹In PDE theory, the Laplacian is a negative operator, while in graph theory it is positive. Therefore it is required to multiply $\hat{\mathbf{L}}$ by a negative sign in Equation (2a) compared to Equation (1).

Namely, the learned parameters are $\boldsymbol{\theta}_a$ the advection parameters, $\boldsymbol{\theta}_d$ the diffusion parameters, and $\boldsymbol{\theta}_r$ the reaction parameters. Therefore, an ADR-GNN layer can express and model various phenomena. For example, if we set $\boldsymbol{\theta}_d(t) = 0$, then there is no diffusion in the system, and the method is dominated by advection and reaction. If on the other hand, one learns a very small advection (i.e., the learned \mathbf{V} , to be discussed later, tends to retain all features in place), then a reaction-diffusion oriented system is obtained. Similarly, other combinations of advection, diffusion, and reaction can be achieved, because of the learning of the parameters of the system. Thus, ADR-GNN can be adopted to solve a host of problems, depending on dynamics and patterns mandated by the data, as we show later in our experiments in Section 4.

3.3 From an ODE to a Graph Neural Network - Time Discretization of ADR-GNN

Equation (2) *spatially* discretizes the PDE in Equation (1), yielding an ODE defined on the graph. The *time* discretization of the ODE yields a sequential process that can be thought of as layers of neural networks (Haber and Ruthotto 2017; Chen et al. 2018b; Weinan 2017). That is, upon discrete time integration of Equation (2a), we replace the notion of time t with l layers, and a step size h , that is a positive scalar hyperparameter.

While it is possible to use many ODE discretization methods (see, e.g., (Haber and Ruthotto 2017; Zhang et al. 2019b; Chen et al. 2018b; Chamberlain et al. 2021) and references within), in various applications where an ADR system arises, from flow in porous media (Coats 2000), to PDE-based image segmentation (Vese and Chan 2002), and multiphase flow (Kadioglu et al. 2011), an operator-splitting (OS) (Ascher 2008) is utilized. We therefore also use an OS time discretization for Equation (2a), that yields a graph neural ADR layer, summarized in Algorithm 1. Composing several neural ADR layers leads to ADR-GNN. We further discuss the properties of the OS approach in Appendix A. The exact discretizations of the ADR terms are derived in Section 3.4.

Algorithm 1: Graph Neural Advection-Diffusion-Reaction Layer

Input: Node features $\mathbf{U}^{(l)} \in \mathbb{R}^{n \times c}$

Output: Updated node features $\mathbf{U}^{(l+1)} \in \mathbb{R}^{n \times c}$

1: Advection:

$$\mathbf{U}^{(l+1/3)} = \mathbf{U}^{(l)} + h\mathbf{DIV}(\mathbf{V}(\mathbf{U}^{(l)}, t; \boldsymbol{\theta}_a^{(l)})\mathbf{U}^{(l)}).$$

2: Diffusion:

$$\mathbf{U}^{(l+2/3)} = \text{mat} \left((\mathbf{I} + h\mathbf{K}(t; \boldsymbol{\theta}_d^{(l)}) \otimes \hat{\mathbf{L}})^{-1} \text{vec}(\mathbf{U}^{(l+1/3)}) \right).$$

3: Reaction:

$$\mathbf{U}^{(l+1)} = \mathbf{U}^{(l+2/3)} + hf(\mathbf{U}^{(l+2/3)}, \mathbf{U}^{(0)}, t; \boldsymbol{\theta}_r^{(l)}).$$

3.4 Discretized Graph Operators

We now elaborate on the discretized graph operators utilized in our ADR-GNN, summarized in Algorithm 1. Besides the combination of the learnable advection, diffusion, and reaction terms, which, to the best of our knowledge, was not studied in the context of GNNs, the main innovation here is

the *consistent, mass preserving, and stable* discretization of the advection operator.

Advection. To define the graph discretized advection operator, we extend the non-learnable advection operator from (Chapman and Chapman 2015), into a learnable, neural advection operator. Our advection operator transports node features based on learned directed edge weights (velocities) $\{(\mathbf{V}_{i \rightarrow j}, \mathbf{V}_{j \rightarrow i})\}_{(i,j) \in \mathcal{E}}$, where each $\mathbf{V}_{i \rightarrow j}, \mathbf{V}_{j \rightarrow i} \in \mathbb{R}^c$, such that $0 \leq \mathbf{V}_{i \rightarrow j} \leq 1$. The notation $i \rightarrow j$ implies that the weight transfers features from the i -th to j -th node. We further demand that the outbound edge weights associated with every node, per channel, sum to 1, i.e., $\sum_{j \in \mathcal{N}_i} \mathbf{V}_{i \rightarrow j} = 1$. This constraint suggests that a node can at most transfer the total of its features to other nodes. First, we define the discretized divergence from Equation (2a), that operates on the learned edge weights \mathbf{V} :

$$\begin{aligned} \text{DIV}_i(\mathbf{V}\mathbf{U}) &= \sum_{j \in \mathcal{N}_i} \mathbf{V}_{j \rightarrow i} \odot \mathbf{U}_j - \mathbf{U}_i \odot \sum_{j \in \mathcal{N}_i} \mathbf{V}_{i \rightarrow j} \\ &= \sum_{j \in \mathcal{N}_i} \mathbf{V}_{j \rightarrow i} \odot \mathbf{U}_j - \mathbf{U}_i, \end{aligned} \quad (4)$$

where \odot is the elementwise Hadamard product. Then, the graph advection operator in Algorithm 1 is:

$$\begin{aligned} \mathbf{U}_i^{(l+1/3)} &= \mathbf{U}_i^{(l)} + h \text{DIV}_i(\mathbf{V}^{(l)} \mathbf{U}^{(l)}) \\ &= \mathbf{U}_i^{(l)} + h \left(\sum_{j \in \mathcal{N}_i} \mathbf{V}_{j \rightarrow i}^{(l)} \odot \mathbf{U}_j^{(l)} - \mathbf{U}_i^{(l)} \right). \end{aligned} \quad (5)$$

Namely, the updated node features are obtained by adding the $\mathbf{V}_{j \rightarrow i}$ weighted inbound node features, while removing the $\mathbf{V}_{i \rightarrow j}$ weighted outbound node features, and h is a positive step size. The scheme in Equation (5) is the forward Euler discretization. We now show that the proposed graph neural advection operator is *mass conserving, stable and consistent*², meaning that our advection operator is adherent to the continuous advection PDE (LeVeque 1990).

Lemma 1 Define the mass of the graph node features $\mathbf{U}^{(l)} \in \mathbb{R}^{n \times c}$ as the scalar $\rho^{(l)} = \sum \mathbf{U}^{(l)}$. Then the advection operator in Equation (5) is mass conserving, i.e., $\rho^{(l+1/3)} = \rho^{(l)}$.

Lemma 2 The advection operator in Equation (5) is stable.

To learn a *consistent* advection operator, i.e., an operator that mimics the directional behavior of the advection in Equation (1), we craft an edge weight \mathbf{V} mechanism, shown in Algorithm 2, that yields direction-oriented weights, i.e., we ensure that $\mathbf{V}_{i \rightarrow j} \neq \mathbf{V}_{j \rightarrow i}$, unless they are zeroes.

Here, $\theta_a^{(l)} = \{\mathbf{A}_1^{(l)}, \mathbf{A}_2^{(l)}, \mathbf{A}_3^{(l)}, \mathbf{A}_4^{(l)}\}$ are learnable fully connected layers, and the exp is computed channel-wise. We note that the sign of $\mathbf{Z}_{ij} - \mathbf{Z}_{ji}$ is opposite than that of $-\mathbf{Z}_{ij} + \mathbf{Z}_{ji}$ in Algorithm 2. Hence, after the $\text{ReLU}(\cdot)$ activation, one of the edge weights, either $\mathbf{V}_{i \rightarrow j}$ or $\mathbf{V}_{j \rightarrow i}$ is guaranteed to be equal to zero, and the other will be non-negative. This allows the architecture to create significant asymmetry in the edge weights \mathbf{V} , as also seen in Figure 1.

Diffusion. To discretize the diffusion term from Equation (2a), both explicit and implicit time discretizations can be

²See stability definition and proofs in Appendix B.

Algorithm 2: Learning directional edge weights.

Input: Node features $\mathbf{U}^{(l)} \in \mathbb{R}^{n \times c}$

Output: Edge weights $\mathbf{V}_{i \rightarrow j}^{(l)}, \mathbf{V}_{j \rightarrow i}^{(l)} \in \mathbb{R}^c$

1: Compute edge features:

$$\mathbf{Z}_{ij}^{(l)} = \text{ReLU}(\mathbf{U}_i^{(l)} \mathbf{A}_1^{(l)} + \mathbf{U}_j^{(l)} \mathbf{A}_2^{(l)}) \mathbf{A}_3^{(l)}.$$

$$\mathbf{Z}_{ji}^{(l)} = \text{ReLU}(\mathbf{U}_j^{(l)} \mathbf{A}_1^{(l)} + \mathbf{U}_i^{(l)} \mathbf{A}_2^{(l)}) \mathbf{A}_3^{(l)}.$$

2: Compute relative edge features:

$$\mathbf{V}_{i \rightarrow j}^{(l)} = \text{ReLU}(\mathbf{Z}_{ij}^{(l)} - \mathbf{Z}_{ji}^{(l)}) \mathbf{A}_4^{(l)}.$$

$$\mathbf{V}_{j \rightarrow i}^{(l)} = \text{ReLU}(-\mathbf{Z}_{ij}^{(l)} + \mathbf{Z}_{ji}^{(l)}) \mathbf{A}_4^{(l)}.$$

3: Normalize to obtain edge weights:

$$\mathbf{V}_{i \rightarrow j}^{(l)} \leftarrow \frac{\exp(\mathbf{V}_{i \rightarrow j}^{(l)})}{\sum_{k \in \mathcal{N}_i} \exp(\mathbf{V}_{i \rightarrow k}^{(l)})}.$$

$$\mathbf{V}_{j \rightarrow i}^{(l)} \leftarrow \frac{\exp(\mathbf{V}_{j \rightarrow i}^{(l)})}{\sum_{k \in \mathcal{N}_j} \exp(\mathbf{V}_{j \rightarrow k}^{(l)})}.$$

used (Ascher 2008). An explicit forward Euler discretization yields the following layer:

$$\mathbf{U}^{(l+2/3)} = \mathbf{U}^{(l+1/3)} - h \left(\hat{\mathbf{L}} \mathbf{U}^{(l+1/3)} \mathbf{K}^{(l)} \right). \quad (6)$$

However, an explicit scheme requires using a small step size $h > 0$, as it is marginally stable (Ascher 2008). We therefore harness an implicit scheme, which guarantees the stability of the diffusion³, and reads:

$$\mathbf{U}^{(l+2/3)} = \text{mat} \left((\mathbf{I} + h \mathbf{K}^{(l)} \otimes \hat{\mathbf{L}})^{-1} \text{vec}(\mathbf{U}^{(l+1/3)}) \right). \quad (7)$$

Here, \otimes is the Kronecker product, $\text{vec}(\cdot)$ is a flattening operator, and $\text{mat}(\cdot)$ reshapes a vector to a matrix. The computation of $\mathbf{U}^{(l+2/3)}$ requires the solution of a linear system, solved by conjugate gradients⁴ (Golub and van Loan 1988; Ascher 2008). In our experiments we found 5 iterations to be sufficient.

Reaction. Our reaction term is realized using MLPs. Recent works showed that utilizing both additive and multiplicative MLPs yields improved performance (Jayakumar et al. 2020; Choi et al. 2022; Ben-Shaul, Galanti, and Dekel 2023). Hence, we define

$$\begin{aligned} f(\mathbf{U}^{(l+2/3)}, \mathbf{U}^{(0)}; \theta_r^{(l)}) &= \sigma(\mathbf{U}^{(l+2/3)} \mathbf{R}_1^{(l)} \\ &+ \tanh(\mathbf{U}^{(l+2/3)} \mathbf{R}_2^{(l)}) \odot \mathbf{U}^{(l+2/3)} + \mathbf{U}^{(0)} \mathbf{R}_3^{(l)}), \end{aligned} \quad (8)$$

as our reaction term in Equation (2a). Here, $\theta_r^{(l)} = \{\mathbf{R}_1^{(l)}, \mathbf{R}_2^{(l)}, \mathbf{R}_3^{(l)}\}$ are trainable fully-connected layers, and σ is non-linear activation function (ReLU in our experiments), that can also be coupled with batch-normalization. This term is integrated via forward Euler as in Algorithm 1.

³See (Koto 2008; Haber et al. 2019; Chamberlain et al. 2021) for details on implicit vs. explicit schemes for diffusion processes and in neural networks.

⁴We note that the matrix $\mathbf{I} + h \mathbf{K}_l \otimes \hat{\mathbf{L}}$ is positive definite and invertible, because the identity matrix is positive definite, h is positive, \mathbf{K}_l is non-negative, and the graph Laplacian $\hat{\mathbf{L}}$ is positive semi-definite.

4 Experimental Results

We demonstrate our ADR-GNN on two types of tasks on real-world datasets: node classification, and spatio-temporal node forecasting. Architectures and training details are provided in Appendix C, and the runtimes and complexity of ADR-GNN are discussed in Appendix D. We use a grid search to select hyperparameters, discussed in Appendix E. Datasets details and statistics are reported in Appendix F. Overall, we propose the two following ADR-GNN architectures:

- ADR-GNN_S. Here we follow a similar approach to typical neural networks, where different weights are learned for each layer. From a dynamical system perspective, this can be interpreted as an unrolled ADR iteration (Mardani et al. 2018). This architecture is suitable for ‘static’ datasets that do not involve temporal information, such as Cora, and is specified in Appendix C.1.
- ADR-GNN_T. A time-dependent ADR-GNN for temporal datasets. Compared to ADR-GNN_S, it also utilizes temporal embedding, discussed in Appendix C.2.

4.1 Node Classification

Homophilic graphs. We experiment with Cora (McCallum et al. 2000), Citeseer (Sen et al. 2008), and Pubmed (Namata et al. 2012) datasets. We use the 10 splits from (Pei et al. 2020) with train/validation/test split ratios of 48%/32%/20%, and report their average accuracy in Table 1. In Appendix G.1 we also provide the accuracy standard deviation. As a comparison, we consider multiple recent methods, such as GCN (Kipf and Welling 2017), GAT (Veličković et al. 2018), Geom-GCN (Pei et al. 2020), APPNP (Klicpera, Bojchevski, and Günnemann 2019), JKNet (Xu et al. 2018), MixHop (Abu-El-Haija et al. 2019), WRGAT (Suresh et al. 2021), GCNII (Ming Chen, Zengfeng Huang, and Li 2020), PDE-GCN (Eliasof, Haber, and Treister 2021), NSD (Bodnar et al. 2022), H2GCN (Zhu et al. 2020b), GGCN (Yan et al. 2022), C&S (Huang et al. 2020), DMP (Yang et al. 2021), GREAD (Choi et al. 2022), LINKX (Lim et al. 2021a), ACMII (Luan et al. 2022), Ord. GNN (Song et al. 2023), and FLODE (Maskey et al. 2023). We see that our ADR-GNN_S outperforms all methods on the Cora and Pubmed datasets, and achieves close (0.12% accuracy difference) to the best performing PDE-GCN on Citeseer.

Heterophilic graphs. While our ADR-GNN offers competitive accuracy on homophilic datasets, as discussed in Section 2, ADR systems are widely used to model non-smooth phenomena and patterns, as often appear in heterophilic datasets by their definition (Pei et al. 2020). We therefore utilize 10 heterophilic datasets from various sources. In Table 2 we compare the average accuracy of our ADR-GNN_S with recent GNNs on the Squirrel, Film, and Chameleon from (Rozemberczki, Allen, and Sarkar 2021), as well as the Cornell, Texas and Wisconsin datasets from (Pei et al. 2020), using the 10-splits from (Pei et al. 2020) we train/validation/test split ratios of 48%/32%/20%. We include more comparisons and the accuracy standard deviation in Appendix G.1. In addition to the previously con-

sidered methods, we also compare with FAGCN (Bo et al. 2021), GraphCON (Rusch et al. 2022a), GPR-GNN (Chien et al. 2021), GRAFF (Giovanni et al. 2023), ACMP-GCN (Wang et al. 2022), and G² (Rusch et al. 2022b). We see that ADR-GNN_S offers accuracy that is in line with recent state-of-the-art methods. In addition, we evaluate ADR-GNN_S on the Twitch-DE, deezer-europe, Penn94, and arXiv-year datasets from (Lim et al. 2021b,a) to further demonstrate the efficacy of our method, in Appendix G.3.

4.2 Spatio-Temporal Node Forecasting

Classical ADR models are widely utilized to predict and model spatio-temporal phenomena (Fiedler and Scheel 2003; Adam and Sibert 2004). We therefore now evaluate our temporal ADR-GNN_T on several spatio-temporal node forecasting datasets. To this end, we harness the software package PyTorch-Geometric-Temporal (Rozemberczki et al. 2021) that offers a graph machine learning pipeline for spatio-temporal graph tasks. In our experiments, we use the Chickenpox Hungary, PedalMe London, and Wikipedia Math datasets from (Rozemberczki et al. 2021), as well as the traffic speed prediction datasets METR-LA (Jagadish et al. 2014) and PEMS-BAY (Chen et al. 2001).

For the first three datasets, we follow the incremental training mode, mean-squared-error (MSE) loss, and testing procedure from (Rozemberczki et al. 2021). We report the performance of ADR-GNN_T and other models, in terms of MSE, in Table 3. We compare with several recent methods, namely, DCRNN (Li et al. 2018), GConv (Seo et al. 2018), GC-LSTM (Chen et al. 2018a), DyGrAE (Taheri, Gimpel, and Berger-Wolf 2019; Taheri and Berger-Wolf 2019), EGCN (Pareja et al. 2020), A3T-GCN (Zhu et al. 2020a), T-GCN (Zhao et al. 2019), MPNN LSTM (Panagopoulos, Nikolentzos, and Vazirgiannis 2021), AGCRN (Bai et al. 2020), and DIFFormer (Wu et al. 2023). Our results in Table 3 show improved performance, further revealing the significance of neural ADR systems on graphs.

On the METR-LA and PEMS-BAY datasets, we follow the same training and testing procedures, and mean-absolute-error (MAE) loss as in (Li et al. 2018). We report the MAE, root mean squared error (RMSE), and mean absolute percentage error (MAPE). To demonstrate the effectiveness of ADR-GNN_T for varying time frame predictions, we report the results on 3, 6, and 12 future frame traffic speed prediction, where each time frame equates to 5 minutes. We compare ADR-GNN_T with various methods, from ‘classical’ approaches such as historical averaging (HA), VAR (Lu et al. 2016), and SVR (Smola and Schölkopf 2004), to neural methods like FC-LSTM (Sutskever, Vinyals, and Le 2014), DCRNN (Li et al. 2018), Graph WaveNet (Wu et al. 2019), ASTGCN (Guo et al. 2019), STSGCN (Song et al. 2020), GMAN (Zheng et al. 2020), MTGNN (Wu et al. 2020), GTS (Shang, Chen, and Bi 2021), STEP (Shao et al. 2022), and STAEformer (Liu et al. 2023). We find that our ADR-GNN_T offers lower (better) metrics than the considered methods. For instance, on METR-LA, ADR-GNN_T reduces the MAE achieved by the recent STEP method from 3.37 to 3.19. We provide the results on METR-LA in Table 4, with additional comparisons as well as results on PEMS-BAY in Appendix

Method	Cora	Citeseer	Pubmed
Homophily	0.81	0.80	0.74
GCN	85.77	73.68	88.13
GAT	86.37	74.32	87.62
GCNII [†]	88.49	77.13	90.30
Geom-GCN [†]	85.27	77.99	90.05
APNP	87.87	76.53	89.40
JKNet	85.25	75.85	88.94
MixHop	87.61	76.26	85.31
WRGAT	88.20	76.81	88.52
PDE-GCN [†]	88.60	78.48	89.93
GRAND	87.36	76.46	89.02
GRAND++	88.15	76.57	88.50
NSD [†]	87.14	77.14	89.49
GGCN	87.95	77.14	89.15
H2GCN	87.87	77.11	89.49
C&S	89.05	76.22	89.74
GRAFF [†]	88.01	77.30	90.04
DMP [†]	86.52	76.87	89.27
GREAD [†]	88.57	77.60	90.23
LINKX	84.64	73.19	87.86
ACMII [†]	88.25	77.12	89.71
Ord. GNN	77.31	90.15	88.37
FLODE	78.07	89.02	86.44
ADR-GNN _S	89.43	78.36	90.55

Table 1: Node accuracy (%) on homophilic datasets.

Method	Squirrel	Film	Chameleon	Cornell	Texas	Wisconsin
Homophily	0.22	0.22	0.23	0.30	0.11	0.21
GCN	23.96	26.86	28.18	52.70	52.16	48.92
GAT	30.03	28.45	42.93	54.32	58.38	49.41
GCNII [†]	38.47	32.87	60.61	74.86	69.46	74.12
Geom-GCN [†]	38.32	31.63	60.90	60.81	67.57	64.12
PDE-GCN [†]	–	–	66.01	89.73	93.24	91.76
GRAND	40.05	35.62	54.67	82.16	75.68	79.41
GRAND++	40.06	33.63	56.20	81.89	77.57	82.75
NSD [†]	56.34	37.79	68.68	86.49	85.95	89.41
GGCN	55.17	37.81	71.14	85.68	84.86	86.86
H2GCN	36.48	35.70	60.11	82.70	84.86	87.65
FAGCN	42.59	34.87	55.22	79.19	82.43	82.94
GPRGNN	31.61	34.63	46.58	80.27	78.38	82.94
GRAFF [†]	59.01	37.11	71.38	84.05	88.38	88.83
DMP [†]	47.26	35.72	62.28	89.19	89.19	92.16
GREAD [†]	59.22	37.90	71.38	87.03	89.73	89.41
ACMP-GCN	–	–	–	85.40	86.20	86.10
LINKX	61.81	36.10	68.42	77.84	74.60	75.49
G ² [†]	64.26	37.30	71.40	87.30	87.57	87.84
ACMII [†]	67.40	37.09	74.76	86.49	88.38	88.43
Ord. GNN	62.44	37.99	72.28	–	–	–
FLODE	64.23	37.16	73.60	–	–	–
ADR-GNN _S	72.54	39.16	79.91	91.89	93.61	93.46

Table 2: Node accuracy (%) on *heterophilic* datasets.

Method	Chickenpox	PedalMe	Wikipedia
DCRNN	1.124 ± 0.015	1.463 ± 0.019	0.679 ± 0.020
GConvGRU	1.128 ± 0.011	1.622 ± 0.032	0.657 ± 0.015
GC-LSTM	1.115 ± 0.014	1.455 ± 0.023	0.779 ± 0.023
DyGrAE	1.120 ± 0.021	1.455 ± 0.031	0.773 ± 0.009
EGCN-O	1.124 ± 0.009	1.491 ± 0.024	0.750 ± 0.014
A3T-GCN	1.114 ± 0.008	1.469 ± 0.027	0.781 ± 0.011
T-GCN	1.117 ± 0.011	1.479 ± 0.012	0.764 ± 0.011
MPNN LSTM	1.116 ± 0.023	1.485 ± 0.028	0.795 ± 0.010
AGCRN	1.120 ± 0.010	1.469 ± 0.030	0.788 ± 0.011
DIFFormer	0.920 ± 0.001	–	0.720 ± 0.036
ADR-GNN _T	0.817 ± 0.012	0.598 ± 0.050	0.571 ± 0.014

Table 3: The performance of spatio-temporal networks evaluated by the average MSE of 10 experimental repetitions and standard deviations, calculated on 10% forecasting horizons.

G.4.

4.3 Ablation Studies

Synthetic Feature Transportation. The benefit of diffusion and reaction are known in GNNs (see (Gasteiger, Weißenberger, and Günnemann 2019; Chamberlain et al. 2021; Choi et al. 2022) and references within). However, the significance of neural advection was not studied in GNNs prior to our work, to the best of our knowledge. Therefore, and following the discussion of the task of feature transportation

in Section 1 and Figure 1, we now compare the behavior of the advection, diffusion, and reaction terms on this task. Although this experiment is conceptually simple, it is evident from Figure 2, that diffusion and reaction terms in GNNs are limited in modeling such a behavior. This result, however, is not surprising. Employing diffusion smooths, rather than directly *transferring* node features. Similarly, the reaction term can only learn to scale the node features in this experiment. On the contrary, Figure 2 that the advection term, that by definition, transports information, achieves an exact fit. More experimental details are given in Appendix G.5.

The Impact of Advection, Diffusion, and Reaction. We study the influence of each of the proposed terms in Equation (2a) on real-world datasets, independently and jointly. The results, reported in Table 5 further show the significance of the advection term. For datasets that are homophilic like Cora, we see minor accuracy improvement when incorporating the advection term. This is in line with known findings regarding the benefits of diffusion for homophilic datasets (Gasteiger, Weißenberger, and Günnemann 2019; Chamberlain et al. 2021). More importantly, we see that mostly for heterophilic datasets like Chameleon, as well as traffic prediction datasets like PEMS-BAY, utilizing the advection significantly improves the performance of the network. Overall, we see that allowing all terms to be learned leads to favorable performance, indicating an implicit balancing of the

Dataset	Method	Horizon 3			Horizon 6			Horizon 12		
		MAE	RMSE	MAPE	MAE	RMSE	MAPE	MAE	RMSE	MAPE
METR -LA	FC-LSTM	3.44	6.30	9.60%	3.77	7.23	10.09%	4.37	8.69	14.00%
	DCRNN	2.77	5.38	7.30%	3.15	6.45	8.80%	3.60	7.60	10.50%
	STGCN	2.88	5.74	7.62%	3.47	7.24	9.57%	4.59	9.40	12.70%
	Graph WaveNet	2.69	5.15	6.90%	3.07	6.22	8.37%	3.53	7.37	10.01%
	ASTGCN	4.86	9.27	9.21%	5.43	10.61	10.13%	6.51	12.52	11.64%
	STSGCN	3.31	7.62	8.06%	4.13	9.77	10.29%	5.06	11.66	12.91%
	GMAN	2.80	5.55	7.41%	3.12	6.49	8.73%	3.44	7.35	10.07%
	MTGNN	2.69	5.18	6.88%	3.05	6.17	8.19%	3.49	7.23	9.87%
	GTS	2.67	5.27	7.21%	3.04	6.25	8.41%	3.46	7.31	9.98%
	STEP	2.61	4.98	6.60%	2.96	5.97	7.96%	3.37	6.99	9.61%
	STAEformer	2.65	5.11	6.85%	2.97	6.00	8.13%	3.34	7.02	9.70%
ADR-GNN _T		2.53	4.85	6.51%	2.81	5.82	7.39%	3.19	6.89	9.10%

Table 4: Multivariate time series forecasting on the METR-LA. Additional results are provided in Appendix G.4.

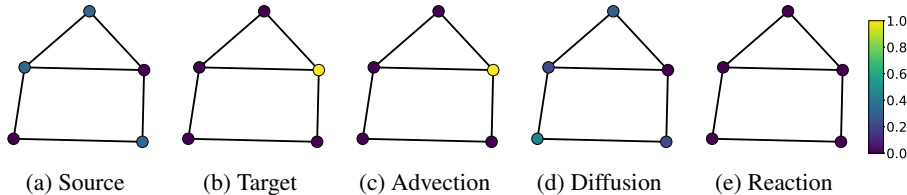


Figure 2: Source and target node features, and their fit using advection, diffusion, and reaction.

terms obtained in the training stage.

The Influence of Number of Layers. The design of ADR-GNN can alleviate oversmoothing in two ways. First, by learning the diffusion coefficients \mathbf{K} , ADR-GNN controls the amount of smoothing, and can also achieve no smoothing if \mathbf{K} is zero, depending on the data. Second, note that the advection and reaction terms can increase the frequency of the node features, because they are not limited to smoothing processes. To verify our observation, we evaluate ADR-GNN_S on Cora and Citeseer with 2 to 64 layers, to see if its performance degrades as more layers are added, an issue that is associated with oversmoothing. We report the obtained accuracy in Figure 3, where no performance drop is evident. For reference, we also report the results obtained with GCN (Kipf and Welling 2017). Also, we define and report the measured Dirichlet energy in Appendix G.6, which shows that ADR-GNN does not oversmooth.

5 Summary and Discussion

In this paper, we present a novel GNN architecture that is based on the Advection-Diffusion-Reaction PDE, called ADR-GNN. We develop a graph neural advection operator that mimics the continuous advection operator, and compose it with learnable diffusion and reaction terms.

We discuss and analyze the properties of ADR-GNN and its flexibility in modeling various phenomena. In particular, we show that the main advantage of the graph advection operator is its ability to transport information over the

A	D	R	Cora	Cham.	METR -LA	PEMS -BAY
✓	✗	✗	86.69	66.79	1.84	3.39
✗	✓	✗	88.21	65.08	1.93	3.67
✗	✗	✓	77.76	52.28	2.19	4.24
✓	✓	✗	88.92	73.33	1.79	3.30
✗	✓	✓	89.33	72.08	1.82	3.46
✓	✗	✓	88.02	73.46	1.71	3.21
✓	✓	✓	89.43	79.91	1.68	3.19

Table 5: Impact of Advection (**A**), Diffusion (**D**), and Reaction (**R**) on the Accuracy (%) on Cora and Chameleon, MAE on METR-LA and PEMS-BAY.

graph edges through the layers - a behavior that is hard to model using the diffusion and reaction terms that have been used in the literature. To demonstrate the effectiveness of ADR-GNN we experiment with total of 18 real-world datasets, from homophilic and heterophilic node classification to spatio-temporal node forecasting datasets.

While the gains observed on homophilic datasets are relatively modest, the performance improvements demonstrated on heterophilic datasets are significant, offering 5% accuracy increase in some cases. Moreover, when applied to spatio-temporal node forecasting datasets, our ADR-GNN exhibits notable enhancements in the evaluated metrics com-

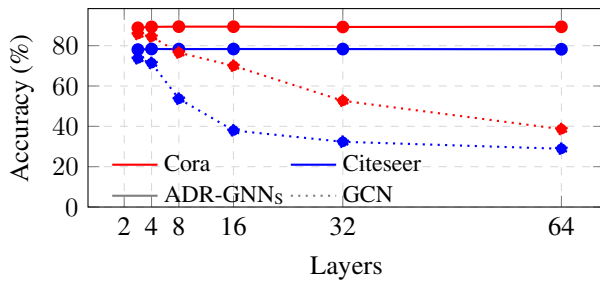


Figure 3: Accuracy (%) vs. model depth.

pared to other methods. This progress can be attributed to the inherent suitability of ADR-GNN for tasks involving directional transportation of features, making it an intuitive choice for modeling such scenarios.

Acknowledgements

This research was supported by grant no. 2018209 from the United States - Israel Binational Science Foundation (BSF), Jerusalem, Israel, and by the Israeli Council for Higher Education (CHE) via the Data Science Research Center and the Lynn and William Frankel Center for Computer Science at BGU. ME is supported by Kreitman High-tech scholarship.

References

Abu-El-Haija, S.; Perozzi, B.; Kapoor, A.; Alipourfard, N.; Lerman, K.; Harutyunyan, H.; Ver Steeg, G.; and Galstyan, A. 2019. Mixhop: Higher-order graph convolutional architectures via sparsified neighborhood mixing. In *international conference on machine learning*, 21–29. PMLR.

Adam, M. S.; and Sibert, J. R. 2004. Use of neural networks with advection-diffusion-reaction models to estimate large-scale movements of Skipjack tuna from tagging data.

Alon, U.; and Yahav, E. 2021. On the Bottleneck of Graph Neural Networks and its Practical Implications. In *International Conference on Learning Representations*.

Ascher, U. M. 2008. *Numerical methods for evolutionary differential equations*. SIAM.

Bai, L.; Yao, L.; Li, C.; Wang, X.; and Wang, C. 2020. Adaptive Graph Convolutional Recurrent Network for Traffic Forecasting. *Advances in Neural Information Processing Systems*, 33.

Belbute-Peres, F. d. A.; Economou, T. D.; and Kolter, J. Z. 2020. Combining Differentiable PDE Solvers and Graph Neural Networks for Fluid Flow Prediction. In *International Conference on Machine Learning (ICML)*.

Ben-Shaul, I.; Galanti, T.; and Dekel, S. 2023. Exploring the Approximation Capabilities of Multiplicative Neural Networks for Smooth Functions. *arXiv preprint arXiv:2301.04605*.

Betts, J. 2001. *Practical Methods for Optimal Control using Nonlinear Programming*. Advances in Design and Control. Philadelphia: SIAM.

Bo, D.; Wang, X.; Shi, C.; and Shen, H. 2021. Beyond Low-frequency Information in Graph Convolutional Networks. In *AAAI*. AAAI Press.

Bodnar, C.; Di Giovanni, F.; Chamberlain, B. P.; Liò, P.; and Bronstein, M. M. 2022. Neural sheaf diffusion: A topological perspective on heterophily and oversmoothing in gnns. *arXiv preprint arXiv:2202.04579*.

Borovitskiy, V.; Azangulov, I.; Terenin, A.; Mostowsky, P.; Deisenroth, M. P.; and Durrande, N. 2021. Matern Gaussian Processes on Graphs. In *International Conference on Artificial Intelligence and Statistics*. PMLR.

Brandstetter, J.; Worrall, D. E.; and Welling, M. 2022. Message Passing Neural PDE Solvers. In *International Conference on Learning Representations*.

Cai, C.; and Wang, Y. 2020. A note on over-smoothing for graph neural networks. *arXiv preprint arXiv:2006.13318*.

Chamberlain, B. P.; Rowbottom, J.; Gorinova, M.; Webb, S.; Rossi, E.; and Bronstein, M. M. 2021. GRAND: Graph neural diffusion. In *International Conference on Machine Learning (ICML)*, 1407–1418. PMLR.

Chapman, A.; and Chapman, A. 2015. Advection on graphs. *Semi-Autonomous Networks: Effective Control of Networked Systems through Protocols, Design, and Modeling*, 3–16.

Chen, C.; Petty, K.; Skabardonis, A.; Varaiya, P.; and Jia, Z. 2001. Freeway performance measurement system: mining loop detector data. *Transportation Research Record*, 1748(1): 96–102.

Chen, D.; Pellizzoni, P.; and Borgwardt, K. 2023. Fisher Information Embedding for Node and Graph Learning. In *International Conference on Machine Learning (ICML)*, Proceedings of Machine Learning Research.

Chen, J.; Xu, X.; Wu, Y.; and Zheng, H. 2018a. GC-LSTM: Graph Convolution Embedded LSTM for Dynamic Link Prediction. *arXiv preprint arXiv:1812.04206*.

Chen, T. Q.; Rubanova, Y.; Bettencourt, J.; and Duvenaud, D. K. 2018b. Neural ordinary differential equations. In *Advances in Neural Information Processing Systems*, 6571–6583.

Chien, E.; Peng, J.; Li, P.; and Milenkovic, O. 2021. Adaptive Universal Generalized PageRank Graph Neural Network. In *International Conference on Learning Representations*.

Choi, J.; Hong, S.; Park, N.; and Cho, S.-B. 2022. GREAD: Graph Neural Reaction-Diffusion Equations. *arXiv preprint arXiv:2211.14208*.

Coats, K. H. 2000. A note on IMPES and some IMPES-based simulation models. *SPE Journal*, 5(03): 245–251.

Cosner, C. 2014. Reaction-diffusion-advection models for the effects and evolution of dispersal. *Discrete & Continuous Dynamical Systems*, 34(5): 1701.

Deepa Maheshvare, M.; Raha, S.; and Pal, D. 2022. A graph-based framework for multiscale modeling of physiological transport. *Frontiers in Network Physiology*, 1: 18.

- Eliasof, M.; Haber, E.; and Treister, E. 2021. PDE-GCN: Novel architectures for graph neural networks motivated by partial differential equations. *Advances in Neural Information Processing Systems*, 34: 3836–3849.
- Evans, L. C. 1998. *Partial Differential Equations*. San Francisco: American Mathematical Society.
- Fiedler, B.; and Scheel, A. 2003. Spatio-temporal dynamics of reaction-diffusion patterns. *Trends in nonlinear analysis*, 23–152.
- Gasteiger, J.; Weißenberger, S.; and Günnemann, S. 2019. Diffusion Improves Graph Learning. In *Conference on Neural Information Processing Systems (NeurIPS)*.
- Giovanni, F. D.; Rowbottom, J.; Chamberlain, B. P.; Markovich, T.; and Bronstein, M. M. 2023. Understanding convolution on graphs via energies. *Transactions on Machine Learning Research*.
- Golub, G.; and van Loan, C. 1988. *Matrix Computations*. Johns Hopkins University Press.
- Gravina, A.; Bacciu, D.; and Gallicchio, C. 2023. Anti-Symmetric DGN: a stable architecture for Deep Graph Networks. In *The Eleventh International Conference on Learning Representations*.
- Gu, F.; Chang, H.; Zhu, W.; Sojoudi, S.; and El Ghaoui, L. 2020. Implicit graph neural networks. *Advances in Neural Information Processing Systems*, 33: 11984–11995.
- Guo, S.; Lin, Y.; Feng, N.; Song, C.; and Wan, H. 2019. Attention based spatial-temporal graph convolutional networks for traffic flow forecasting. In *Proceedings of the AAAI conference on artificial intelligence*, volume 33, 922–929.
- Haber, E. 2014. *Computational Methods in Geophysical Electromagnetics*. Philadelphia: SIAM.
- Haber, E.; Lensink, K.; Treister, E.; and Ruthotto, L. 2019. IMEXnet a forward stable deep neural network. In *International Conference on Machine Learning*, 2525–2534. PMLR.
- Haber, E.; and Ruthotto, L. 2017. Stable architectures for deep neural networks. *Inverse Problems*, 34(1).
- Hochbruck, M.; Luibich, C.; and Selhofer, H. 1998. Exponential integrators for large systems of differential equations. *SIAM J. Sci. Comp.*, 19. N5.
- Hošek, R.; and Volek, J. 2019. Discrete advection–diffusion equations on graphs: Maximum principle and finite volumes. *Applied Mathematics and Computation*, 361: 630–644.
- Huang, Q.; He, H.; Singh, A.; Lim, S.-N.; and Benson, A. R. 2020. Combining label propagation and simple models out-performs graph neural networks. *arXiv preprint arXiv:2010.13993*.
- Jagadish, H. V.; Gehrke, J.; Labrinidis, A.; Papakonstantinou, Y.; Patel, J. M.; Ramakrishnan, R.; and Shahabi, C. 2014. Big data and its technical challenges. *Communications of the ACM*, 57(7): 86–94.
- Jayakumar, S. M.; Czarnecki, W. M.; Menick, J.; Schwarz, J.; Rae, J.; Osindero, S.; Teh, Y. W.; Harley, T.; and Pascanu, R. 2020. Multiplicative Interactions and Where to Find Them. In *International Conference on Learning Representations*.
- Kadioglu, S.; Knoll, D.; Sussman, M.; and Martineau, R. 2011. A second order JFNK-based IMEX method for single and multi-phase flows. In *Computational Fluid Dynamics 2010*, 549–554. Springer.
- Khokhlov, A. M. 1995. Propagation of turbulent flames in supernovae. *The Astrophysical Journal*, 449: 695.
- Kipf, T. N.; and Welling, M. 2017. Semi-supervised classification with graph convolutional networks. *International Conference on Learning Representations (ICLR)*.
- Klicpera, J.; Bojchevski, A.; and Günnemann, S. 2019. Combining Neural Networks with Personalized PageRank for Classification on Graphs. In *International Conference on Learning Representations*.
- Koto, T. 2008. IMEX Runge–Kutta schemes for reaction–diffusion equations. *Journal of Computational and Applied Mathematics*, 215(1): 182–195.
- LeVeque, R. 1990. *Numerical Methods for Conservation Laws*. Birkhauser.
- Li, Y.; Yu, R.; Shahabi, C.; and Liu, Y. 2018. Diffusion Convolutional Recurrent Neural Network: Data-Driven Traffic Forecasting. In *International Conference on Learning Representations*.
- Li, Z.; Kovachki, N.; Azizzadenesheli, K.; Liu, B.; Stuart, A.; Bhattacharya, K.; and Anandkumar, A. 2020. Multipole graph neural operator for parametric partial differential equations. *Advances in Neural Information Processing Systems*, 33: 6755–6766.
- Lim, D.; Hohne, F. M.; Li, X.; Huang, S. L.; Gupta, V.; Bhalerao, O. P.; and Lim, S.-N. 2021a. Large Scale Learning on Non-Homophilous Graphs: New Benchmarks and Strong Simple Methods. In Beygelzimer, A.; Dauphin, Y.; Liang, P.; and Vaughan, J. W., eds., *Advances in Neural Information Processing Systems*.
- Lim, D.; Li, X.; Hohne, F.; and Lim, S.-N. 2021b. New Benchmarks for Learning on Non-Homophilous Graphs. *Workshop on Graph Learning Benchmarks, WWW*.
- Liu, H.; Dong, Z.; Jiang, R.; Deng, J.; Deng, J.; Chen, Q.; and Song, X. 2023. Spatio-temporal adaptive embedding makes vanilla transformer sota for traffic forecasting. In *Proceedings of the 32nd ACM International Conference on Information and Knowledge Management*, 4125–4129.
- Long, Z.; Lu, Y.; Ma, X.; and Dong, B. 2018. PDE-Net: Learning PDEs from Data.
- Lu, Z.; Zhou, C.; Wu, J.; Jiang, H.; and Cui, S. 2016. Integrating granger causality and vector auto-regression for traffic prediction of large-scale WLANs. *KSII Transactions on Internet and Information Systems (TIIS)*, 10(1): 136–151.
- Luan, S.; Hua, C.; Lu, Q.; Zhu, J.; Zhao, M.; Zhang, S.; Chang, X.-W.; and Precup, D. 2022. Revisiting Heterophily For Graph Neural Networks. *Conference on Neural Information Processing Systems*.
- Luan, S.; Zhao, M.; Hua, C.; Chang, X.-W.; and Precup, D. 2020. Complete the missing half: Augmenting aggregation filtering with diversification for graph convolutional networks. *arXiv preprint arXiv:2008.08844*.

- Mardani, M.; Sun, Q.; Donoho, D.; Pappayan, V.; Monajemi, H.; Vasanawala, S.; and Pauly, J. 2018. Neural proximal gradient descent for compressive imaging. *Advances in Neural Information Processing Systems*, 31.
- Maskey, S.; Paolino, R.; Bacho, A.; and Kutyniok, G. 2023. A Fractional Graph Laplacian Approach to Oversmoothing. In *Thirty-seventh Conference on Neural Information Processing Systems*.
- Mattheij, R. M.; Rienstra, S. W.; and Boonkkamp, J. T. T. 2005. *Partial differential equations: modeling, analysis, computation*. SIAM.
- McCallum, A. K.; Nigam, K.; Rennie, J.; and Seymore, K. 2000. Automating the construction of internet portals with machine learning. *Information Retrieval*, 3(2): 127–163.
- Ming Chen, Z. W.; Zengfeng Huang, B. D.; and Li, Y. 2020. Simple and Deep Graph Convolutional Networks.
- Namata, G.; London, B.; Getoor, L.; Huang, B.; and Edu, U. 2012. Query-driven active surveying for collective classification. In *10th International Workshop on Mining and Learning with Graphs*, volume 8, 1.
- Nt, H.; and Maehara, T. 2019. Revisiting graph neural networks: All we have is low-pass filters. *arXiv preprint arXiv:1905.09550*.
- Oono, K.; and Suzuki, T. 2020. Graph Neural Networks Exponentially Lose Expressive Power for Node Classification. In *International Conference on Learning Representations*.
- Panagopoulos, G.; Nikolentzos, G.; and Vazirgiannis, M. 2021. Transfer Graph Neural Networks for Pandemic Forecasting. In *Proceedings of the 35th AAAI Conference on Artificial Intelligence*.
- Pareja, A.; Domeniconi, G.; Chen, J.; Ma, T.; Suzumura, T.; Kanezashi, H.; Kaler, T.; Schardl, T. B.; and Leiserson, C. E. 2020. EvolveGCN: Evolving Graph Convolutional Networks for Dynamic Graphs. In *AAAI*, 5363–5370.
- Pei, H.; Wei, B.; Chang, K. C.-C.; Lei, Y.; and Yang, B. 2020. Geom-GCN: Geometric Graph Convolutional Networks. In *International Conference on Learning Representations*.
- Raissi, M. 2018. Deep hidden physics models: Deep learning of nonlinear partial differential equations. *The Journal of Machine Learning Research*, 19(1): 932–955.
- Rozemberczki, B.; Allen, C.; and Sarkar, R. 2021. Multi-Scale Attributed Node Embedding. *Journal of Complex Networks*, 9(2).
- Rozemberczki, B.; Scherer, P.; He, Y.; Panagopoulos, G.; Riedel, A.; Astefanoaei, M.; Kiss, O.; Beres, F.; López, G.; Collignon, N.; et al. 2021. Pytorch geometric temporal: Spatiotemporal signal processing with neural machine learning models. In *Proceedings of the 30th ACM International Conference on Information & Knowledge Management*, 4564–4573.
- Rusch, T. K.; Bronstein, M. M.; and Mishra, S. 2023. A Survey on Oversmoothing in Graph Neural Networks. *arXiv preprint arXiv:2303.10993*.
- Rusch, T. K.; Chamberlain, B.; Rowbottom, J.; Mishra, S.; and Bronstein, M. 2022a. Graph-coupled oscillator networks. In *International Conference on Machine Learning*, 18888–18909. PMLR.
- Rusch, T. K.; Chamberlain, B. P.; Mahoney, M. W.; Bronstein, M. M.; and Mishra, S. 2022b. Gradient Gating for Deep Multi-Rate Learning on Graphs. *arXiv preprint arXiv:2210.00513*.
- Ruthotto, L.; and Haber, E. 2020. Deep neural networks motivated by partial differential equations. *Journal of Mathematical Imaging and Vision*, 62: 352–364.
- Saadat, M.; Gjorgiev, B.; Das, L.; and Sansavini, G. 2022. Neural tangent kernel analysis of PINN for advection-diffusion equation. *arXiv preprint arXiv:2211.11716*.
- Sanchez-Gonzalez, A.; Bapst, V.; Cranmer, K.; and Battaglia, P. 2019. Hamiltonian graph networks with ode integrators. *arXiv preprint arXiv:1909.12790*.
- Seed, A. 2003. A dynamic and spatial scaling approach to advection forecasting. *Journal of Applied Meteorology and Climatology*, 42(3): 381–388.
- Sen, P.; Namata, G.; Bilgic, M.; Getoor, L.; Galligher, B.; and Eliassi-Rad, T. 2008. Collective classification in network data. *AI magazine*, 29(3): 93–93.
- Seo, Y.; Defferrard, M.; Vandergheynst, P.; and Bresson, X. 2018. Structured Sequence Modeling with Graph Convolutional Recurrent Networks. In *International Conference on Neural Information Processing*, 362–373. Springer.
- Shang, C.; Chen, J.; and Bi, J. 2021. Discrete Graph Structure Learning for Forecasting Multiple Time Series. In *International Conference on Learning Representations*.
- Shao, Z.; Zhang, Z.; Wang, F.; and Xu, Y. 2022. Pre-training enhanced spatial-temporal graph neural network for multivariate time series forecasting. In *Proceedings of the 28th ACM SIGKDD Conference on Knowledge Discovery and Data Mining*, 1567–1577.
- Smola, A. J.; and Schölkopf, B. 2004. A tutorial on support vector regression. *Statistics and computing*, 14: 199–222.
- Song, C.; Lin, Y.; Guo, S.; and Wan, H. 2020. Spatial-temporal synchronous graph convolutional networks: A new framework for spatial-temporal network data forecasting. In *Proceedings of the AAAI conference on artificial intelligence*, volume 34, 914–921.
- Song, Y.; Zhou, C.; Wang, X.; and Lin, Z. 2023. Ordered GNN: Ordering Message Passing to Deal with Heterophily and Over-smoothing. In *The Eleventh International Conference on Learning Representations*.
- Suresh, S.; Budde, V.; Neville, J.; Li, P.; and Ma, J. 2021. Breaking the Limit of Graph Neural Networks by Improving the Assortativity of Graphs with Local Mixing Patterns. *Proceedings of the 27th ACM SIGKDD Conference on Knowledge Discovery & Data Mining*.
- Sutskever, I.; Vinyals, O.; and Le, Q. V. 2014. Sequence to sequence learning with neural networks. *Advances in neural information processing systems*, 27.
- Taheri, A.; and Berger-Wolf, T. 2019. Predictive Temporal Embedding of Dynamic Graphs. In *Proceedings of the 2019*

- IEEE/ACM International Conference on Advances in Social Networks Analysis and Mining*, 57–64.
- Taheri, A.; Gimpel, K.; and Berger-Wolf, T. 2019. Learning to Represent the Evolution of Dynamic Graphs with Recurrent Models. In *Companion Proceedings of The 2019 World Wide Web Conference*, WWW '19, 301–307.
- Thorpe, M.; Nguyen, T. M.; Xia, H.; Strohmer, T.; Bertozzi, A.; Osher, S.; and Wang, B. 2022. GRAND++: Graph Neural Diffusion with A Source Term. In *International Conference on Learning Representations*.
- Uys, L. 2009. *Coupling kinetic models and advection-diffusion equations to model vascular transport in plants, applied to sucrose accumulation in sugarcane*. Ph.D. thesis, Stellenbosch: University of Stellenbosch.
- Veličković, P.; Cucurull, G.; Casanova, A.; Romero, A.; Liò, P.; and Bengio, Y. 2018. Graph Attention Networks. *International Conference on Learning Representations*.
- Vese, L. A.; and Chan, T. F. 2002. A multiphase level set framework for image segmentation using the Mumford and Shah model. *International journal of computer vision*, 50(3): 271–293.
- Wang, Y.; Yi, K.; Liu, X.; Wang, Y. G.; and Jin, S. 2022. ACMP: Allen-Cahn Message Passing for Graph Neural Networks with Particle Phase Transition. *arXiv preprint arXiv:2206.05437*.
- Weinan, E. 2017. A Proposal on Machine Learning via Dynamical Systems. *Communications in Mathematics and Statistics*, 5(1): 1–11.
- Wu, Q.; Yang, C.; Zhao, W.; He, Y.; Wipf, D.; and Yan, J. 2023. DIFFormer: Scalable (Graph) Transformers Induced by Energy Constrained Diffusion. In *The Eleventh International Conference on Learning Representations*.
- Wu, Z.; Pan, S.; Long, G.; Jiang, J.; Chang, X.; and Zhang, C. 2020. Connecting the dots: Multivariate time series forecasting with graph neural networks. In *Proceedings of the 26th ACM SIGKDD international conference on knowledge discovery & data mining*, 753–763.
- Wu, Z.; Pan, S.; Long, G.; Jiang, J.; and Zhang, C. 2019. Graph Wavenet for Deep Spatial-Temporal Graph Modeling. In *Proceedings of the 28th International Joint Conference on Artificial Intelligence*, IJCAI'19, 1907–1913. AAAI Press. ISBN 9780999241141.
- Xu, K.; Li, C.; Tian, Y.; Sonobe, T.; Kawarabayashi, K.-i.; and Jegelka, S. 2018. Representation Learning on Graphs with Jumping Knowledge Networks. In Dy, J.; and Krause, A., eds., *Proceedings of the 35th International Conference on Machine Learning*, volume 80 of *Proceedings of Machine Learning Research*, 5453–5462. PMLR.
- Yan, Y.; Hashemi, M.; Swersky, K.; Yang, Y.; and Koutra, D. 2022. Two sides of the same coin: Heterophily and over-smoothing in graph convolutional neural networks. In *2022 IEEE International Conference on Data Mining (ICDM)*, 1287–1292. IEEE.
- Yang, L.; Li, M.; Liu, L.; Wang, C.; Cao, X.; Guo, Y.; et al. 2021. Diverse message passing for attribute with heterophily. *Advances in Neural Information Processing Systems*, 34: 4751–4763.
- Zhang, K.; Hao, M.; Wang, J.; de Silva, C. W.; and Fu, C. 2019a. Linked dynamic graph CNN: Learning on point cloud via linking hierarchical features. *arXiv preprint arXiv:1904.10014*.
- Zhang, T.; Yao, Z.; Gholami, A.; Gonzalez, J. E.; Keutzer, K.; Mahoney, M. W.; and Biros, G. 2019b. ANODEV2: A coupled neural ODE framework. *Advances in Neural Information Processing Systems*, 32.
- Zhao, J.; Dong, Y.; Ding, M.; Kharlamov, E.; and Tang, J. 2021. Adaptive Diffusion in Graph Neural Networks. In Beygelzimer, A.; Dauphin, Y.; Liang, P.; and Vaughan, J. W., eds., *Advances in Neural Information Processing Systems*.
- Zhao, L.; Song, Y.; Zhang, C.; Liu, Y.; Wang, P.; Lin, T.; Deng, M.; and Li, H. 2019. T-GCN: A Temporal Graph Convolutional Network for Traffic Prediction. *IEEE Transactions on Intelligent Transportation Systems*, 21(9): 3848–3858.
- Zheng, C.; Fan, X.; Wang, C.; and Qi, J. 2020. Gman: A graph multi-attention network for traffic prediction. In *Proceedings of the AAAI conference on artificial intelligence*, volume 34, 1234–1241.
- Zheng, Y.; Zhang, H.; Lee, V. C.; Zheng, Y.; Wang, X.; and Pan, S. 2023. Finding the Missing-Half: Graph Complementary Learning for Homophily-Prone and Heterophily-Prone Graphs. In *Proceedings of the 40th International Conference on Machine Learning*, ICML'23. JMLR.org.
- Zhu, J.; Song, Y.; Zhao, L.; and Li, H. 2020a. A3T-GCN: Attention Temporal Graph Convolutional Network for Traffic Forecasting. *arXiv preprint arXiv:2006.11583*.
- Zhu, J.; Yan, Y.; Zhao, L.; Heimann, M.; Akoglu, L.; and Koutra, D. 2020b. Beyond homophily in graph neural networks: Current limitations and effective designs. *Advances in Neural Information Processing Systems*, 33: 7793–7804.
- Zhuang, J.; Dvornik, N.; Li, X.; and Duncan, J. S. 2020. Ordinary differential equations on graph networks.

A The Behavior of the Operator Splitting Approach

The advantage of Operator Splitting (OS) is that it allows the individual treatment of each component of the ODE separately, thus obtaining the appropriate qualitative behavior. This is especially beneficial in the context of advection, where it is difficult to obtain stability, that is, to satisfy the CFL condition (LeVeque 1990), as well as to obtain mass conservation. Furthermore, OS is beneficial for the diffusion component, where implicit methods guarantee stability (Ascher 2008) compared to unstable explicit discretizations.

We now discuss the behavior of the OS approach for integrating the ADR ODE in Equation (2). The theory behind OS can be analyzed in the linear case, and in the case of non-linear equations, linearization is typically assumed (Mattheij, Rienstra, and Boonkkamp 2005). We now consider a linear ODE of the form

$$\frac{d\mathbf{U}(t)}{dt} = \mathbf{A}\mathbf{U} + \mathbf{D}\mathbf{U} + \mathbf{R}\mathbf{U}, \quad (9)$$

where \mathbf{A} , \mathbf{D} , \mathbf{R} denote the advection, diffusion, and reaction operators, respectively. $\mathbf{U}(t)$ denotes the node features at time t .

Suppose that we are interested in computing $\mathbf{U}(t + \delta t)$. For this constant ODE system, the *analytic*, exact solution is given by (Evans 1998):

$$\mathbf{U}(t + \delta t) = \exp(\delta t(\mathbf{A} + \mathbf{D} + \mathbf{R})) \mathbf{U}(t). \quad (10)$$

The following Lemma is easily proven using Taylor series of the matrix exponential function (Ascher 2008):

Lemma 3 *Let $\mathbf{Q} = \exp(\delta t(\mathbf{A} + \mathbf{D} + \mathbf{R}))$ where \mathbf{A} , \mathbf{D} , and \mathbf{R} are matrices that do not share their eigenvectors. Then the discrepancy between the exact and OS solution operator reads*

$$\mathbf{Q} - \exp(\delta t\mathbf{R})\exp(\delta t\mathbf{D})\exp(\delta t\mathbf{A}) = \mathcal{O}(\delta t^2)$$

Remark 1 *If the eigenvectors of \mathbf{A} , \mathbf{D} , \mathbf{R} from Lemma 3 are shared, then the matrix exponents commute, and the discrepancy is zero.*

Following Lemma 3, it holds that the solution of the ADR ODE can be expressed as a sequential process of three separate problems, with an error of $\mathcal{O}(\delta t^2)$ compared to the exact solution, as follows:

$$\exp(\delta t(\mathbf{A} + \mathbf{D} + \mathbf{R})) \mathbf{U}(t) \quad (11)$$

$$= \exp(\delta t\mathbf{R})\exp(\delta t\mathbf{D})\exp(\delta t\mathbf{A}) \mathbf{U}(t) + \mathcal{O}(\delta t^2) \quad (12)$$

$$= \exp(\delta t\mathbf{R}) \underbrace{(\exp(\delta t\mathbf{D}) (\exp(\delta t\mathbf{A}) \mathbf{U}(t)))}_{\text{Advection}} + \mathcal{O}(\delta t^2) \quad (13)$$

$$\underbrace{\underbrace{\underbrace{\exp(\delta t\mathbf{R}) \exp(\delta t\mathbf{D}) \exp(\delta t\mathbf{A})}_{\text{Advection-Diffusion}}}_{\text{Advection-Diffusion-Reaction}}}_{\text{Advection-Diffusion-Reaction}}$$

Note that $\mathbf{U}^{(l+1/3)} = \exp(\delta t\mathbf{A})\mathbf{U}^{(l)}$ is the exact solution (Hochbruck, Luibich, and Selhofer 1998) of the reaction system $\frac{d\mathbf{U}(t)}{dt} = \mathbf{A}\mathbf{U}$. Similarly, $\mathbf{U}^{(l+2/3)} = \exp(\delta t\mathbf{D})\mathbf{U}^{(l+1/3)}$ is the exact solution of the diffusion system $\frac{d\mathbf{U}(t)}{dt} = \mathbf{D}\mathbf{U}$, and $\mathbf{U}^{(l+1)} = \exp(\delta t\mathbf{R})\mathbf{U}^{(l+2/3)}$ is the

exact solution of the reaction system $\frac{d\mathbf{U}(t)}{dt} = \mathbf{R}\mathbf{U}$. Thus, operator splitting can be viewed as taking a step of advection, followed by a step of diffusion that is finally followed by a reaction step. Note that the error above is of the same magnitude as each step of the forward Euler integration scheme, often used in neural networks, e.g., in ResNet (see [A] in additional references below).

B The Properties of the Graph Discretized Advection Operator

In this section, we prove Lemma 1 and Lemma 2 from the main text. For convenience, we repeat the Lemmas, followed by their proofs. We start by noting the following remark:

Remark 2 *The advection operator in Equation (5) does not mix the node feature \mathbf{U} channels in our ADR-GNN.*

The importance of this remark is that it allows us to analyze the properties of the advection operator per-channel, or, alternatively, assuming a single channel, $c = 1$, which we assume in our following proofs.

Lemma 1 *Define the mass of the graph node features $\mathbf{U}^{(l)} \in \mathbb{R}^{n \times c}$ as the scalar $\rho^{(l)} = \sum \mathbf{U}^{(l)}$. Then the advection operator in Equation (5) is mass conserving, i.e., $\rho^{(l+1/3)} = \rho^{(l)}$.*

Proof 1 *Without loss of generality, and following Remark 2, let us assume a single channel, and consider the mass of the node features $\rho = \sum \mathbf{U}$, before and after applying an advection layer as described in Equation (5). The input node features has a total mass of $\rho^{(l)} = \sum \mathbf{U}^{(l)}$. The total mass of the output of an advection layer reads:*

$$\rho^{(l+1/3)} \quad (14a)$$

$$= \sum_i \mathbf{U}_i^{(l+1/3)} \quad (14b)$$

$$= \sum_i \left(\mathbf{U}_i^{(l)} + h \sum_{j \in \mathcal{N}_i} \mathbf{V}_{j \rightarrow i}^{(l)} \mathbf{U}_j^{(l)} - h \mathbf{U}_i^{(l)} \right) \quad (14c)$$

$$= \sum_i \left(\mathbf{U}_i^{(l)} + h \sum_j \mathbf{V}_{j \rightarrow i}^{(l)} \mathbf{U}_j^{(l)} - h \mathbf{U}_i^{(l)} \right) \quad (14d)$$

$$= \sum_i \mathbf{U}_i^{(l)} + h \left(\sum_i \sum_j \mathbf{U}_j^{(l)} (\mathbf{V}_{j \rightarrow i}^{(l)}) - \sum_i \mathbf{U}_i^{(l)} \right) \quad (14e)$$

$$= \sum_i \mathbf{U}_i^{(l)} + h \left(\sum_j \mathbf{U}_j^{(l)} \left(\sum_i \mathbf{V}_{j \rightarrow i}^{(l)} \right) - \sum_i \mathbf{U}_i^{(l)} \right) \quad (14f)$$

$$= \sum_i \mathbf{U}_i^{(l)} + h \left(\sum_j \mathbf{U}_j^{(l)} - \sum_i \mathbf{U}_i^{(l)} \right) \quad (14g)$$

$$= \sum_i \mathbf{U}_i^{(l)} = \rho^{(l)}. \quad (14h)$$

The transition between Equations (14c) and (14d) is valid because for $j \notin \mathcal{N}_i$, the edge weight is zero, i.e., $\mathbf{V}_{j \rightarrow i}^{(l)} = 0$, and therefore the summation does not change. Also, the transition between Equations (14f) and (14h) holds because of the constraint on the sum of outbound edge weights to be equal to 1, i.e. $\sum_{i \in \mathcal{N}_j} \mathbf{V}_{j \rightarrow i}^{(l)} = 1$. Therefore, because

$\rho^{(l+1/3)} = \rho^{(l)}$, our graph discretized advection operator is mass preserving.

Definition 1 A neural operator F that considers node features \mathbf{U} is (Lyapunov) stable if for every $\epsilon > 0$ there exists $\delta > 0$, such that every pair of inputs $\mathbf{U}, \tilde{\mathbf{U}}$ that satisfy $\|\mathbf{U} - \tilde{\mathbf{U}}\| \leq \delta$, then $\|F(\mathbf{U}) - F(\tilde{\mathbf{U}})\| \leq \epsilon$.

Lemma 2 The advection operator in Equation (5) is stable.

Proof 2 Without loss of generality, and following Remark 2, let us consider a single channel, and let $\mathbf{V}^{(l)}$ be a sparse matrix such that $\mathbf{V}_{ij}^{(l)} = \mathbf{V}_{i \rightarrow j}^{(l)}$. To show stability, we first observe that the matrix form of the scalar formulation of the advection layer in Equation (5) is given by:

$$\mathbf{U}^{(l+1/3)} = \mathbf{I}\mathbf{U}^{(l)} + h\mathbf{V}^{(l)}\mathbf{U}^{(l)} - h\mathbf{U}^{(l)} \quad (15)$$

$$= \underbrace{\left((1-h)\mathbf{I} + h\mathbf{V}^{(l)} \right)}_{\mathbf{A}^{(l)}} \mathbf{U}^{(l)}. \quad (16)$$

Because of the demand that $\mathbf{V}^{(l)}$ is normalized (i.e., $\sum_{j \in \mathcal{N}_i} \mathbf{V}_{i \rightarrow j}^{(l)} = 1$), and the advection weights satisfy $0 \leq \mathbf{V}_{i \rightarrow j}^{(l)} \leq 1$, the advection operator $\mathbf{A}^{(l)}$ is a column stochastic non-negative matrix. By the Perron-Frobenius theorem, such matrices are known to have a spectral radius bounded by 1 (see [B] in additional appendix references), and hence the advection operator is stable.

C Architectures and Training Details

As discussed in the main paper, we propose two architectures, depending on the type of dataset - static (e.g., Cora), or spatio-temporal (e.g., PEMS-BAY). In the following subsections, we elaborate on these architectures.

C.1 Node Classification: ADR-GNN_S

We now elaborate on the ‘static’ architecture ADR-GNN_S used in our node classification experiments. The overall architecture is similar to standard GNN architectures for node classification, such as GCN (Kipf and Welling 2017) and GCNII (Ming Chen, Zengfeng Huang, and Li 2020). It is composed of an initial embedding layer (that corresponds to Equation (2b) in the main paper), L graph neural ADR layers, and a classifier, as described in Equation (3) in the main paper. The complete flow of ADR-GNN_S is described in Algorithm 3. To train ADR-GNN_S on node classification datasets, we minimize the cross-entropy loss between the ground-truth node labels \mathbf{Y} and the predicted node labels $\hat{\mathbf{Y}}$, as is standard in GNNs, and similar to (Kipf and Welling 2017).

C.2 Spatio-Temporal Node Forecasting: ADR-GNN_T

The typical task in spatio-temporal datasets is to predict future quantities (e.g., driving speed) given several previous time steps (also called frames). Formally, one is given an input tensor $\mathbf{X}_{temporal} \in \mathbb{R}^{n \times \tau_{in} \times c_{in}}$, where τ_{in} is the number of input (observed) time frames, and the goal is to predict τ_{out} time frames ahead, i.e., $\mathbf{Y}_{temporal} \in \mathbb{R}^{n \times \tau_{out} \times c_{out}}$.

This is in contrast to ‘static’ datasets such as Cora (McCallum et al. 2000), where input node features $\mathbf{X} \in \mathbb{R}^{n \times c_{in}}$ are given, and the goal is to fit to some ground-truth $\mathbf{Y} \in \mathbb{R}^{n \times c_{out}}$. In this context, a ‘static’ dataset can be thought of as setting $\tau_{in} = \tau_{out} = 1$ for the spatio-temporal settings. We show the overall flow of our ‘temporal’ architecture ADR-GNN_T in Algorithm 4⁵.

In our spatio-temporal ADR-GNN_T, we update the hidden state feature matrix $\mathbf{U}_{state}^{(l)}$ based on the hidden historical feature matrix $\mathbf{U}_{hist}^{(l)}$, as shown in Lines 6-9 in Algorithm 4.

Similarly to Attention models (see [C] in the additional appendix references), we incorporate time embedding based on the concatenation of sine and cosine function evaluations with varying frequencies multiplied by the time of the input frames, as input to our ADR-GNN_T, denoted by $\mathbf{T}_{emb} \in \mathbb{R}^{n \times \tau_{in} \times c_t}$, where we choose the number of frequencies to be 10, and by the concatenation of both sine and cosine lead to $c_t = 20$. We note that the time embedding is computed in a pre-processing fashion. To initialize the hidden feature matrices $\mathbf{U}_{state}^{(0)}, \mathbf{U}_{hist}^{(0)}$, we embed the input data $\mathbf{X}_{temporal}$, concatenated with \mathbf{T}_{emb} , using two fully connected layers, as described in Lines 3-4 in Algorithm 4.⁶

For the Chickenpox Hungary, PedalMe London, and Wikipedia Math datasets, we minimize the mean squared error (MSE) between the ground truth future node quantities and the predicted quantities by ADR-GNN_T, similar to the training procedure of the rest of the considered methods in Table 3. Specifically, following (Rozemberczki et al. 2021), the goal is to predict the node quantities of the next time frame given 4 previous time frames. On the METR-LA and PEMS-BAY datasets we minimize the mean absolute error (MAE), similar to (Li et al. 2018), where we also follow the standard 12 previous time frames as inputs, and consider 3,6, and 12 future time frames node quantity prediction as output.

D Computational Complexity and Time

Complexity. Our ADR-GNN architectures include four main operations: (i) input/output embedding, (ii) advection, (iii) diffusion, and (iv) reaction layers.

The complexity of (i) and (iv) is $\mathcal{O}(|\mathcal{V}|c^2)$, where c is the number of channels, because they are composed of point-wise MLPs. The complexity of (ii) is $\mathcal{O}((|\mathcal{V}| + |\mathcal{E}|)c^2)$ because it requires the computation of the edge weights \mathbf{V} , as shown in Algorithm 2, followed by a multiplication by the node features, as shown in Equation (5). Similarly, (iii) also is of complexity $\mathcal{O}((|\mathcal{V}| + |\mathcal{E}|)c)$, because it is required to multiply the scaled Laplacian with the node features. Note that as discussed in Section 3.4, and similar to (Chamberlain et al. 2021; Rusch et al. 2022a), we do not explicitly invert the matrix $\mathbf{I} + h\mathbf{K}^{(l)} \otimes \hat{\mathbf{L}}$, but rather use the conjugate-gradients (CG) method to solve a system of equations. Below, we further discuss the use of CG to solve the system of

⁵In Algorithm 4, \oplus denotes channel-wise concatenation.

⁶In Python notations, $\mathbf{X}_{temporal}[:, -c_{in}]$ extracts the last c_{in} entries of the second dimension of $\mathbf{X}_{temporal}$, which returns the features of the last time frame.

Algorithm 3: ADR-GNN_S Architecture Flow

Input: Node features $\mathbf{X} \in \mathbb{R}^{n \times c_{in}}$
Output: Predicted node labels $\tilde{\mathbf{Y}} \in \mathbb{R}^{n \times c_{out}}$

- 1: **procedure** ADR-GNN_S
- 2: $\mathbf{X} \leftarrow \text{Dropout}(\mathbf{X}, p)$
- 3: $\mathbf{U}^{(0)} = g_{in}(\mathbf{X})$
- 4: **for** $l = 0 \dots L - 1$ **do**
- 5: $\mathbf{U}^{(l)} \leftarrow \text{Dropout}(\mathbf{U}^{(l)}, p)$
- 6: Advection: $\mathbf{U}^{(l+1/3)} = \mathbf{U}^{(l)} + h\text{DIV}(\mathbf{V}(\mathbf{U}^{(l)}; \boldsymbol{\theta}_a^{(l)})\mathbf{U}^{(l)})$
- 7: Diffusion: $\mathbf{U}^{(l+2/3)} = \text{mat}\left(\left(\mathbf{I} + h\mathbf{K}(\boldsymbol{\theta}_d^{(l)}) \otimes \hat{\mathbf{L}}\right)^{-1}\text{vec}(\mathbf{U}^{(l+1/3)})\right)$
- 8: Reaction: $\mathbf{U}^{(l+1)} = \mathbf{U}^{(l+2/3)} + hf(\mathbf{U}^{(l+2/3)}, \mathbf{U}^{(0)}; \boldsymbol{\theta}_r^{(l)})$
- 9: **end for**
- 10: $\mathbf{U}^{(L)} \leftarrow \text{Dropout}(\mathbf{U}^{(L)}, p)$
- 11: $\tilde{\mathbf{Y}} = g_{out}(\mathbf{U}^{(L)})$
- 12: Return $\tilde{\mathbf{Y}}$
- 13: **end procedure**

equations.

Implicit solution of the diffusion term. The diffusion step in our ADR-GNN, as shown in Section 3.4, requires the solution of the linear system at each step. As previously discussed this is solved by using the CG method. Thus, the backward (differentiation) function in most common software packages, such as PyTorch, tracks the CG iterations. This tracking can be avoidable by using implicit differentiation, which is the backbone of implicit methods (see (Haber 2014) for detailed derivation). In the context of deep learning, implicit differentiation was used for implicit neural networks (Gu et al. 2020). The basic idea is to use implicit differentiation of the equation

$$\mathbf{U}^{(l+2/3)} = \text{mat}\left(\left(\mathbf{I} - h\mathbf{K}^{(l)} \otimes \hat{\mathbf{L}}\right)\text{vec}(\mathbf{U}^{(l+1/3)})\right) \quad (17)$$

with respect to $\mathbf{K}^{(l)}$ and thus avoid the tracking of the CG iterations if many are needed.

Runtimes. In addition to the complexity analysis above, we provide the measured runtimes in Table 6. Learning the advection weights requires an increased computational effort. However, it can significantly improve the considered task metric. For convenience, in Table 6, in addition to the runtimes we also report the obtained task metric. Importantly, we show that the improved metrics offered by ADR-GNN_S with 64 channels and 4 layers are not simply obtained due to the increased costs, by showing that enlarging GCN and GAT from standard 2 layers and 64 channels, to 2 layers and 256 channels (wide), or 64 layers and 64 channels (deep) does not yield similar improvements. We measure the runtimes using an Nvidia-RTX3090 with 24GB of memory, which is the same GPU used to conduct our experiments.

E Hyperparameters

All hyperparameters were determined by grid search, and the ranges and sampling mechanism distributions are provided in Table 7. Note, that as discussed after Equation (8), we may add a BatchNorm layer before applying the non-

linear activation σ to the reaction term, we therefore treat the use of batchnorm as a hyperparameter in Table 7.

F Datasets

We report the statistics of the datasets used in our experiments in Table 8 and 9 for the node classification, and spatio-temporal node forecasting datasets, respectively. All datasets are publicly available, and appropriate references to the data sources are provided in the main paper.

G Experimental Results

G.1 Additional Comparisons and Standard Deviations on Node Classification

To allow a more comprehensive comparison, and because some of the considered methods did not report the standard deviation around the mean accuracy, we now provide the experimental results from 4.1 on Cora, Citeseer, Pubmed datasets in Table 10, and Cornell, Texas, Wisconsin, Squirrel, Film, Chameleon datasets in Table 11, with the standard deviation around the mean of the 10 splits from (Pei et al. 2020). Note, that here we do not color the tables, because some of the second or third top performing models in the main paper did not report the accuracy standard deviation, and therefore coloring Tables 10-11 will change the order of the best performing models.

G.2 Large Scale Homophilic Node Classification

We evaluate our ADR-GNN_S on the OGBN-Arxiv dataset and compare it with several methods such as GCN, GRAND, FIE (Chen, Pellizzoni, and Borgwardt 2023), GOAL (Zheng et al. 2023), and ADGN (Zhao et al. 2021), in Table 12. The results further indicate the efficacy of ADR-GNN_S on large scale homophilic node classification cases.

Algorithm 4: ADR-GNN_T Architecture Flow

Input: Node features $\mathbf{X}_{\text{temporal}} \in \mathbb{R}^{n \times \tau_{in} c_{in}}$, time embedding $\mathbf{T}_{\text{emb}} \in \mathbb{R}^{n \times \tau_{in} c_t}$
Output: Predicted future node quantities $\tilde{\mathbf{Y}} \in \mathbb{R}^{n \times \tau_{out} c_{out}}$

- 1: **procedure** ADR-GNN_T
- 2: $\mathbf{X}_{\text{temporal}} \leftarrow \text{Dropout}(\mathbf{X}_{\text{temporal}}, p)$
- 3: $\mathbf{T}_{\text{emb}} \leftarrow \text{g}^{\text{time-embed}}(\mathbf{T}_{\text{emb}})$
- 4: $\mathbf{U}_{\text{state}}^{(0)} = g_{in}^{\text{state}}(\mathbf{X}_{\text{temporal}}[:, -c_{in}] \oplus \mathbf{T}_{\text{emb}})$
- 5: $\mathbf{U}_{\text{hist}}^{(0)} = g_{in}^{\text{hist}}(\mathbf{X}_{\text{temporal}} \oplus \mathbf{T}_{\text{emb}})$
- 6: **for** $l = 0 \dots L - 1$ **do**
- 7: $\mathbf{U}_{\text{state}}^{(l)} \leftarrow \text{Dropout}(\mathbf{U}_{\text{state}}^{(l)}, p)$
- 8: Advection: $\mathbf{U}_{\text{state}}^{(l+1/3)} = \mathbf{U}_{\text{state}}^{(l)} + h\text{DIV}(\mathbf{V}(\mathbf{U}_{\text{hist}}^{(l)}; \boldsymbol{\theta}_a^{(l)})\mathbf{U}_{\text{state}}^{(l)}, \boldsymbol{\theta}_a)\mathbf{U}_{\text{state}}^{(l)}$
- 9: Diffusion: $\mathbf{U}_{\text{state}}^{(l+2/3)} = \text{mat}\left(\left(\mathbf{I} + h\mathbf{K}^{(l)} \otimes \hat{\mathbf{L}}\right)^{-1} \text{vec}(\mathbf{U}_{\text{state}}^{(l+1/3)})\right)$
- 10: Reaction: $\mathbf{U}_{\text{state}}^{(l+1)} = \mathbf{U}_{\text{state}}^{(l+2/3)} + hf(\mathbf{U}_{\text{hist}}^{(l+2/3)}, \mathbf{U}_{\text{hist}}^{(0)}; \boldsymbol{\theta}_r)$
- 11: $\mathbf{U}_{\text{hist}}^{(l+1)} = g_l^{\text{hist}}(\mathbf{U}_{\text{hist}}^{(l)} \oplus \mathbf{U}_{\text{state}}^{(l+1)} \oplus \mathbf{T}_{\text{emb}})$
- 12: **end for**
- 13: $\mathbf{U}_{\text{state}}^{(L)} \leftarrow \text{Dropout}(\mathbf{U}_{\text{state}}^{(L)}, p)$
- 14: $\tilde{\mathbf{Y}} = g_{out}^{\text{state}}(\mathbf{U}_{\text{state}}^{(L)})$
- 15: Return $\tilde{\mathbf{Y}}$
- 16: **end procedure**

Table 6: Training and inference GPU runtimes (milliseconds), number of parameters (thousands), and node classification accuracy (%) on Cora.

Metric	GCN	GAT	GCN (wide)	GAT (wide)	GCN (deep)	GAT (deep)	ADR-GNN _S
Training time	7.71	14.59	14.32	36.63	95.11	184.51	35.41
Inference time	1.75	2.98	2.86	7.57	12.93	38.96	8.24
Parameters	104	105	565	567	358	360	210
Accuracy	85.77	83.13	85.18	83.37	38.62	33.40	89.43

G.3 Additional Heterophilic Node Classification Datasets

In addition to the 6 heterophilic node classification datasets reported in the main paper in Section 4.1, we now also report the results on 4 additional heterophilic datasets from (Lim et al. 2021b,a), to further demonstrate the effectiveness of our ADR-GNN_S. The results are reported in Table 13, where we see that our ADR-GNN_S achieves competitive results that are in line or better than other recent methods. In addition to the methods considered in the main paper, here we also consider SGC ([D] in the additional appendix references), L prop ([E]), and LINK (Lim et al. 2021b).

G.4 Spatio-Temporal Node Forecasting Results

We provide here full results of our spatio-temporal experiments, both on the METR-LA and PEMS-BAY datasets. In addition, we also include results with 'classical' algorithms such as HA (historic averaging), VAR, and SVR. The results are reported in Table 14.

G.5 Synthetic Experiment

We now provide the details of the construction of the synthetic experiment from our ablation study in Section 4.3 in the main paper. The experiment is conducted as follows: we generate a random Erdős-Rényi graph $\mathcal{G}_{\text{ER}} = (\mathcal{E}_{\text{ER}}, \mathcal{V}_{\text{ER}})$, and randomly select a set of *source* nodes $\mathcal{V}_{\text{ER}}^{\text{src}} \subset \mathcal{V}_{\text{ER}}$ assigned with value of $\frac{1}{|\mathcal{V}_{\text{ER}}^{\text{src}}|}$. The rest of the nodes $\mathcal{V}_{\text{ER}} \setminus \mathcal{V}_{\text{ER}}^{\text{src}}$ are initialized with a value of 0. We also choose a random node $\mathbf{v}_{\text{dst}} \in \mathcal{V}_{\text{ER}} \setminus \mathcal{V}_{\text{ER}}^{\text{src}}$. The goal is to transport all the mass from all the nodes to the \mathbf{v}_{dst} , such that \mathbf{v}_{dst} will have a feature of 1, the the rest of the nodes in the graph will be zeroes. That is, all the features in the graph are concentrated in \mathbf{v}_{dst} . In our example in Figure 2, we use the protocol specified here, to generate a graph with 5 nodes, and we show the approximation obtained with the advection, diffusion, and reaction terms.

Table 7: Hyperparameter ranges

Hyperparameter	Range	Uniform Distribution
input/output embedding learning rate	[1e-4, 1e-1]	log uniform
advection learning rate	[1e-4, 1e-1]	log uniform
diffusion learning rate	[1e-4, 1e-1]	log uniform
reaction learning rate	[1e-4, 1e-1]	log uniform
input/output embedding weight decay	[0, 1e-2]	uniform
advection weight decay	[0, 1e-2]	uniform
diffusion weight decay	[0, 1e-2]	uniform
reaction weight decay	[0, 1e-2]	uniform
input/output dropout	[0, 0.9]	uniform
hidden layer dropout	[0, 0.9]	uniform
use BatchNorm	{ yes / no }	discrete uniform
step size h	[1e-3, 1]	uniform
layers	{ 2,4,8,16,32,64 }	discrete uniform
channels	{ 8,16,32,64,128,256 }	discrete uniform

Table 8: Node classification datasets statistics.

Dataset	Classes	Nodes	Edges	Features	Homophily
Cora	7	2,708	5,429	1,433	0.81
Citeseer	6	3,327	4,732	3,703	0.80
Pubmed	3	19,717	44,338	500	0.74
Chameleon	5	2,277	36,101	2,325	0.23
Film	5	7,600	33,544	932	0.22
Squirrel	5	5,201	198,493	2,089	0.22
Cornell	5	183	295	1,703	0.30
Texas	5	183	309	1,703	0.11
Wisconsin	5	251	499	1,703	0.21
Twitch-DE	2	9,498	76,569	2,545	0.63
Deezer-Europe	2	28,281	92,752	31,241	0.52
Penn94 (FB100)	2	41,554	1,362,229	5	0.47
arXiv-year	5	169,343	1,166,243	128	0.22
OGBN-Arxiv	40	169,343	1,166,243	128	0.65

G.6 The Dirichlet Energy of ADR-GNN

We follow (Rusch et al. 2022b) and define the Dirichlet energy of the graph node features as:

$$E(\mathbf{U}^{(l)}) = \frac{1}{|\mathcal{V}|} \sum_{i \in \mathcal{V}} \sum_{j \in \mathcal{N}_i} \|\mathbf{U}_i^{(l)} - \mathbf{U}_j^{(l)}\|_2^2. \quad (18)$$

Following the experiment in our ablation study in Section 4.3, we now also report the measured Dirichlet energy of our ADR-GNN_s on Cora and Citeseer, with 64 layers. We also compare the measured Dirichlet energy of GCN, for reference. The results are reported in Figure 4, where we show the relative (to the initial node features $\mathbf{U}^{(0)}$) Dirichlet energy. It is evident that ADR-GNN_s does not oversmooth, because the energy does not decay to 0, as in GCN.

Table 9: Attributes of the spatio-temporal datasets used in 4.2 and information about the number of time periods (T) and spatial units ($|\mathcal{V}|$).

Dataset	Frequency	T	$ \mathcal{V} $
Chickenpox Hungary	Weekly	522	20
Pedal Me Deliveries	Weekly	36	15
Wikipedia Math	Daily	731	1,068
METR-LA	5-Minutes	34,272	207
PEMS-BAY	5-Minutes	52,116	325

Table 10: Node classification accuracy (%) on *homophilic* datasets. † denotes the maximal accuracy of several proposed variants.

Method	Cora	Citeseer	Pubmed
Homophily	0.81	0.80	0.74
GCN	85.77 ± 1.27	73.68 ± 1.36	88.13 ± 0.50
GAT	86.37 ± 0.48	74.32 ± 1.23	87.62 ± 1.10
GCNII†	88.49 ± 1.25	77.13 ± 1.48	90.30 ± 0.43
Geom-GCN†	85.27 ± 1.57	77.99 ± 1.15	90.05 ± 0.47
MixHop	87.61 ± 2.03	76.26 ± 2.95	85.31 ± 2.29
WRGAT	88.20 ± 2.26	76.81 ± 1.89	88.52 ± 0.92
NSD†	87.14 ± 1.13	77.14 ± 1.57	89.49 ± 0.40
GGCN	87.95 ± 1.05	77.14 ± 1.45	89.15 ± 0.37
H2GCN	87.87 ± 1.20	77.11 ± 1.57	89.49 ± 0.38
LINKX	84.64 ± 1.13	73.19 ± 0.99	87.86 ± 0.77
ACMII-GCN++	88.25 ± 0.96	77.12 ± 1.58	89.71 ± 0.48
ADR-GNN _S	89.43 ± 1.15	78.36 ± 1.44	90.55 ± 0.53

Table 11: Node classification accuracy (%) on *heterophilic* datasets. † denotes the maximal accuracy of several proposed variants.

Method	Squirrel	Film	Cham.	Corn.	Texas	Wisc.
Homophily	0.22	0.22	0.23	0.30	0.11	0.21
GCN	23.96 ± 2.01	26.86 ± 1.10	28.18 ± 2.24	52.70 ± 5.30	52.16 ± 5.16	48.92 ± 3.06
GAT	30.03 ± 1.55	28.45 ± 0.89	42.93 ± 2.50	54.32 ± 5.05	58.38 ± 6.63	49.41 ± 4.09
GCNII	38.47 ± 1.58	32.87 ± 1.30	60.61 ± 3.04	74.86 ± 3.79	69.46 ± 3.83	74.12 ± 3.40
Geom-GCN†	38.32 ± 0.92	31.63 ± 1.15	60.90 ± 2.81	60.81 ± 3.67	67.57 ± 2.72	64.12 ± 3.66
MixHop	43.80 ± 1.48	32.22 ± 2.34	60.50 ± 2.53	73.51 ± 6.34	77.84 ± 7.73	75.88 ± 4.90
GRAND	40.05 ± 1.50	35.62 ± 1.01	54.67 ± 2.54	82.16 ± 7.09	75.68 ± 7.25	79.41 ± 3.64
NSD†	56.34 ± 1.32	37.79 ± 1.15	68.68 ± 1.58	86.49 ± 4.71	85.95 ± 5.51	89.41 ± 4.74
WRGAT	48.85 ± 0.78	36.53 ± 0.77	65.24 ± 0.87	81.62 ± 3.90	83.62 ± 5.50	86.98 ± 3.78
MagNet	–	–	–	84.30 ± 7.00	83.30 ± 6.10	85.70 ± 3.20
GGCN	55.17 ± 1.58	37.81 ± 1.56	71.14 ± 1.84	85.68 ± 6.63	84.86 ± 4.55	86.86 ± 3.29
H2GCN	36.48 ± 1.86	35.70 ± 1.00	60.11 ± 1.71	82.70 ± 5.28	84.86 ± 7.23	87.65 ± 4.98
GraphCON†	–	–	–	84.30 ± 4.80	85.40 ± 4.20	87.80 ± 3.30
FAGCN	42.59 ± 0.69	34.87 ± 1.35	55.22 ± 2.11	79.19 ± 5.87	82.43 ± 2.87	82.94 ± 1.58
GPRGNN	31.61 ± 1.24	34.63 ± 1.22	46.58 ± 1.71	80.27 ± 8.11	78.38 ± 4.36	82.94 ± 4.21
ACMP-GCN	–	–	–	85.40 ± 7.00	86.20 ± 3.00	86.10 ± 4.00
LINKX	61.81 ± 1.80	36.10 ± 1.55	68.42 ± 1.38	77.84 ± 5.81	74.60 ± 8.37	75.49 ± 5.72
GRAFF†	59.01 ± 1.31	37.11 ± 1.08	71.38 ± 1.47	84.05 ± 6.10	88.38 ± 4.53	88.83 ± 3.29
G ² †	64.26 ± 2.38	37.30 ± 1.01	71.40 ± 2.38	87.30 ± 4.84	87.57 ± 3.86	87.84 ± 3.49
ACMII-GCN++	67.40 ± 2.21	37.09 ± 1.32	74.76 ± 2.20	86.49 ± 6.73	88.38 ± 3.43	88.43 ± 3.66
ADR-GNN _S	72.54 ± 2.20	39.16 ± 1.13	79.91 ± 2.27	91.89 ± 5.89	93.61 ± 4.26	93.46 ± 4.11

Table 12: Node classification accuracy (%) on OGBN-Arxiv.

Method	GCN	GRAND	FIE	GOAL	AGDN	ADR-GNN _S
Accuracy (%)	71.74	72.23	72.39	71.25	73.41	73.68

Table 13: Test accuracy on heterophilic datasets. For all datasets, we report the obtained accuracy (%), besides Twitch-DE that considers test ROC AUC_‡. Standard deviations are over 5 train/val/test splits. Not available results are indicated by –.

Method	Twitch-DE _‡	Deezer-Europe	Penn94 (FB100)	arXiv-year
MLP	69.20 ± 0.62	66.55 ± 0.72	73.61 ± 0.40	36.70 ± 0.21
L Prop (2 hop)	72.27 ± 0.78	56.96 ± 0.26	74.13 ± 0.46	46.07 ± 0.15
LINK	72.42 ± 0.57	57.71 ± 0.36	80.79 ± 0.49	53.97 ± 0.18
LINKX	–	–	84.41 ± 0.52	56.00 ± 1.34
SGC (2 hop)	73.65 ± 0.40	61.56 ± 0.51	76.09 ± 0.45	32.27 ± 0.06
C&S (2 hop)	69.39 ± 0.85	64.52 ± 0.62	72.47 ± 0.73	42.17 ± 0.27
GCN	74.07 ± 0.68	62.23 ± 0.53	82.47 ± 0.27	46.02 ± 0.26
GAT	73.13 ± 0.29	61.09 ± 0.77	81.53 ± 0.55	46.05 ± 0.51
APPNP	72.20 ± 0.73	67.21 ± 0.56	74.95 ± 0.45	38.15 ± 0.26
H2GCN	72.67 ± 0.65	67.22 ± 0.90	–	49.09 ± 0.10
GCNII	72.38 ± 0.31	66.42 ± 0.56	82.92 ± 0.59	47.21 ± 0.28
MixHop	73.23 ± 0.99	66.80 ± 0.58	83.47 ± 0.71	51.81 ± 0.17
GPR-GNN	73.84 ± 0.69	66.90 ± 0.50	84.59 ± 0.29	45.07 ± 0.21
ACMII [†]	–	67.50 ± 0.53	85.95 ± 0.26	–
G ²	–	–	–	63.30 ± 1.84
ADR-GNN _S	74.98 ± 0.52	68.22 ± 0.57	86.63 ± 0.31	61.17 ± 1.54

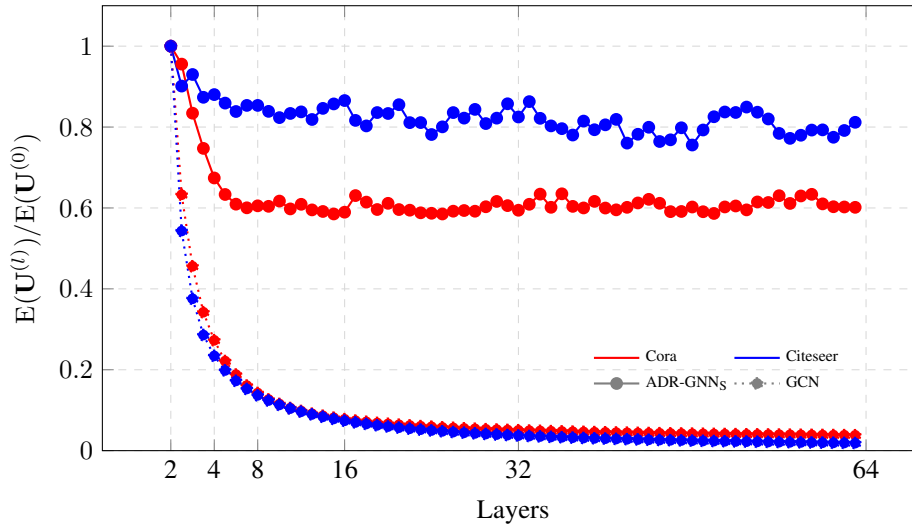


Figure 4: The relative Dirichlet energy vs. model depth.

Dataset	Method	Horizon 3			Horizon 6			Horizon 12		
		MAE	RMSE	MAPE	MAE	RMSE	MAPE	MAE	RMSE	MAPE
METR -LA	HA	4.79	10.00	11.70%	5.47	11.45	13.50%	6.99	13.89	17.54%
	VAR	4.42	7.80	13.00%	5.41	9.13	12.70%	6.52	10.11	15.80%
	SVR	3.39	8.45	9.30%	5.05	10.87	12.10%	6.72	13.76	16.70%
	FC-LSTM	3.44	6.30	9.60%	3.77	7.23	10.09%	4.37	8.69	14.00%
	DCRNN	2.77	5.38	7.30%	3.15	6.45	8.80%	3.60	7.60	10.50%
	STGCN	2.88	5.74	7.62%	3.47	7.24	9.57%	4.59	9.40	12.70%
	Graph WaveNet	2.69	5.15	6.90%	3.07	6.22	8.37%	3.53	7.37	10.01%
	ASTGCN	4.86	9.27	9.21%	5.43	10.61	10.13%	6.51	12.52	11.64%
	STSGCN	3.31	7.62	8.06%	4.13	9.77	10.29%	5.06	11.66	12.91%
	GMAN	2.80	5.55	7.41%	3.12	6.49	8.73%	3.44	7.35	10.07%
	MTGNN	2.69	5.18	6.88%	3.05	6.17	8.19%	3.49	7.23	9.87%
	GTS	2.67	5.27	7.21%	3.04	6.25	8.41%	3.46	7.31	9.98%
	STEP	2.61	4.98	6.60%	2.96	5.97	7.96%	3.37	6.99	9.61%
	STAEformer	2.65	5.11	6.85%	2.97	6.00	8.13%	3.34	7.02	9.70%
ADR-GNN _T		2.53	4.85	6.51%	2.81	5.82	7.39%	3.19	6.89	9.10%
PEMS -BAY	HA	1.89	4.30	4.16%	2.50	5.82	5.62%	3.31	7.54	7.65%
	VAR	1.74	3.16	3.60%	2.32	4.25	5.00%	2.93	5.44	6.50%
	SVR	1.85	3.59	3.80%	2.48	5.18	5.50%	3.28	7.08	8.00%
	FC-LSTM	2.05	4.19	4.80%	2.20	4.55	5.20%	2.37	4.96	5.70%
	DCRNN	1.38	2.95	2.90%	1.74	3.97	3.90%	2.07	4.74	4.90%
	STGCN	1.36	2.96	2.90%	1.81	4.27	4.17%	2.49	5.69	5.79%
	Graph WaveNet	1.30	2.74	2.73%	1.63	3.70	3.67%	1.95	4.52	4.63%
	ASTGCN	1.52	3.13	3.22%	2.01	4.27	4.48%	2.61	5.42	6.00%
	STSGCN	1.44	3.01	3.04%	1.83	4.18	4.17%	2.26	5.21	5.40%
	GMAN	1.34	2.91	2.86%	1.63	3.76	3.68%	1.86	4.32	4.37%
	GTS	1.34	2.83	2.82%	1.66	3.78	3.77%	1.95	4.43	4.58%
	STEP	1.26	2.73	2.59%	1.55	3.58	3.43%	1.79	4.20	4.18%
	STAEformer	1.31	2.78	2.76%	1.62	3.68	3.62%	1.88	4.34	4.41%
	ADR-GNN _T		1.13	2.36	2.30%	1.39	3.13	3.01%	1.68	3.81

Table 14: Multivariate time series forecasting on the METR-LA, and PEMS-BAY datasets.

Additional Appendix References

[A] Kaiming He, Xiangyu Zhang, Shaoqing Ren, and Jian Sun. Deep residual learning for image recognition. In Proceedings of the IEEE Conference on Computer Vision and Pattern Recognition, pages 770–778, 2016.

[B] R. A. Horn and C. R. Johnson. Matrix Analysis. Academic Press, 1985.

[C] Ashish Vaswani, Noam Shazeer, Niki Parmar, Jakob Uszkoreit, Llion Jones, Aidan N Gomez, Łukasz Kaiser, and Illia Polosukhin. Attention is all you need. Advances in neural information processing systems, 30, 2017.

[D] Felix Wu, Amauri Souza, Tianyi Zhang, Christopher Fifty, Tao Yu, and Kilian Weinberger. Simplifying graph convolutional networks. In International conference on machine learning, pages 6861–6871. PMLR, 2019.

[E] Leto Peel. Graph-based semi-supervised learning for relational networks. In Proceedings of 910 the 2017 SIAM international conference on data mining, pages 435–443. SIAM, 2017.

This figure "dynamics.png" is available in "png" format from:

<http://arxiv.org/ps/2307.16092v2>